Journal of Building Engineering 43 (2021) 102563

Contents lists available at ScienceDirect

Journal of Building Engineering

journal homepage: www.elsevier.com/locate/jobe

Elastic drift amplification factor in steel moment frames with double reduced beam section (DRBS) connections

Nader Fanaie [a,*], Zahra Nadalipour [a], Omid Sepasgozar Sarkhosh [b], Shervin Safaei Faegh [a]

[a] Faculty of Civil Engineering, K. N. Toosi University of Technology, Tehran, Iran
[b] Department of Civil Engineering, Faculty of Engineering, University of Guilan, Rasht, Iran

ARTICLE INFO

Keywords:
Reduced beam section
Steel moment frames
Elastic drift amplification factor
Method of virtual work
Response surface method

ABSTRACT

The recently proposed double reduced beam section (DRBS) connection is a steel moment connection intended to delay buckling failure modes and achieve a more ductile seismic behavior. This design adds an extra reduced section to the prequalified radius-cut reduced beam section (RBS) connection and aims to shift the plastic hinge further away from the beam-column interface. In this study, to investigate the effect of the DRBS connection on the stiffness of the steel moment frames, first, while presenting a theoretical approach based on geometric relationships and utilizing the method of virtual work, the exact formulae for calculating the elastic drift and the elastic drift amplification factor in a steel moment frame with DRBS connections were developed. Next, by conducting a sensitivity analysis, the DRBS connection parameters with the most significant effect on the elastic drift of the considered frame were determined. The accuracy of the proposed exact theoretical formulae and the conducted sensitivity analysis was confirmed through finite element modeling. The response surface method (RSM) was then utilized to derive highly accurate and specific relationships for the elastic drift amplification factor in frames made of the different HEA and IPE sections considered. Ultimately, two accurate and simple formulae based on the DRBS connection parameters were presented for estimating the elastic drift amplification factor in steel moment frames with DRBS connections constructed of HEA and IPE sections. The results indicated that utilizing DRBS connections could increase the elastic drift up to 14.7% and 5.5% in steel moment frames built with HEA and IPE sections, respectively.

1. Introduction

Prior to the 1994 Northridge and 1995 Kobe earthquakes, the most common type of beam-to-column connection used in steel moment frames was the connection of beam flanges to column flange using complete joint penetration (CJP) groove welds [1]. Nevertheless, the structures with such connections sustained severe damages during the earthquakes mentioned. These widespread failures mainly occurred due to the formation of a plastic joint in the connection region and near the column face [2]. Hence, the inherent inability of simple moment connections to provide sufficient ductility became evident [3]. The high concentration of stress in the flange and web welds and the vulnerability of the connection to large ductility demands have been identified as two critical factors in the observed failures [1].

The seismic resistance of a steel moment frame is highly dependent on the type and quality of the connection used for joining the beams and columns [2]. Hence, to achieve a better seismic performance, the demand for ductility in the weld zones must be reduced [1]. Two main approaches have been suggested to address this issue; The first one is adding some elements to the connection to increase beam strength and reduce the stress in the connection. The second one is weakening the beam at a specific distance from the connection so that less moment and shear is transferred to the connection.

Among the new designs proposed, the reduced beam section (RBS) connection showed satisfactory results in multiple experiments and became widely accepted. In the RBS connection, parts of the beam flanges are strategically reduced at a short distance from the column face. The original geometry for this design, proposed by Plumier [4], was the straight-cut (trapezoidal) RBS connection with a necked-down transition region. Chen et al. [5], considering the seismic moment profile in beams, suggested that tapered-cut RBS connections be used instead of the original design to facilitate uniform yielding of flanges at the reduced section. However, both the straight-cut and the tapered-cut geometries could lead to stress concentration at the reentrant corners of the resulting RBS profile. To minimize such stress concentration,

* Corresponding author. Faculty of Civil Engineering, K. N. Toosi University of Technology, No. 1346, Valiasr St., PO Box 15875-4416, Tehran, Iran.
E-mail address: fanaie@kntu.ac.ir (N. Fanaie).

https://doi.org/10.1016/j.jobe.2021.102563
Received 14 January 2021; Received in revised form 15 March 2021; Accepted 14 April 2021
Available online 18 April 2021

Nomenclature

a	The distance between the column face and the start of the reduced section in the RBS connection
a_1	The distance between the column face and the start of the first reduced section in the DRBS connection
a_2	The distance between the end of the first reduced section and the start of the second reduced section in the DRBS connection
A_c	Cross-sectional area of the column
A_s	Shear cross-sectional area of the beam or column
b	Length of the reduced section in the RBS connection
b_1	Length of the first reduced section in the DRBS connection
b_2	Length of the second reduced section in the DRBS connection
b_f	Flange width
b_{RBS}	Flange width in the middle of the reduced section in the RBS connection
c	Depth of the reduced section in the RBS connection
c_1	Depth of the first reduced section in the DRBS connection
c_2	Depth of the second reduced section in the DRBS connection
d_b	Beam section depth
E	Modulus of elasticity
G	Shear modulus
h_w	Web height
H	Beam or column section height
I_b	Moment of inertia of the beam section
I_C	Moment of inertia of the column section
L_b	Beam length
L_c	Column length
M	Internal bending moment
P	Lateral shear force applied to the moment frame
R	Radius of the cut in the RBS connection
R_1	Radius of the first cut in the DRBS connection
R_2	Radius of the second cut in the DRBS connection
t_f	Flange thickness
t_w	Web thickness
Δ	Translational displacement
ν	Poisson's ratio

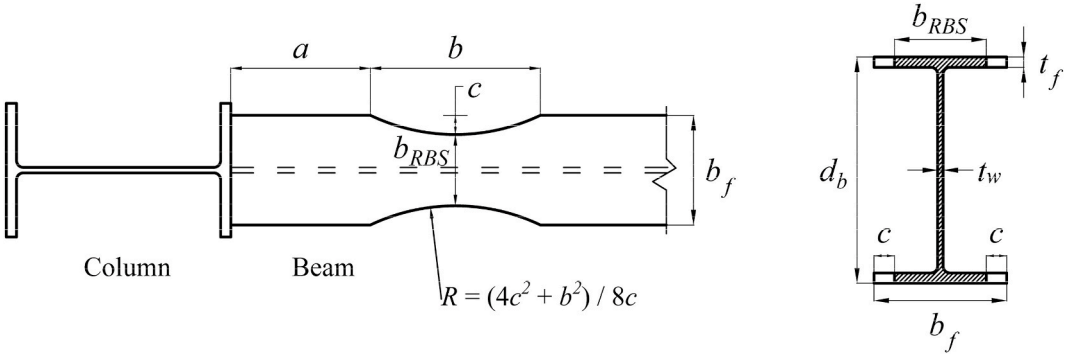

Fig. 1. Typical geometry of the radius-cut RBS connection.

Engelhardt et al. [6] proposed the radius-cut RBS connection (Fig. 1). This concept was also independently suggested by other researchers, including Plumier [7] and Popov et al. [8].

The reduction of the flange width near the connections in special moment frames is currently regarded as an acceptable alteration to improve seismic performance. In RBS connections, the beam flanges are connected to the column flange by CJP groove welds. The beam web is also connected to the column flange via either a CJP groove weld or bolts. The nonlinear behavior of the frames with RBS connections indicates that these connections lead to improved performance curves, more ductile behavior, and a reduction in strain concentration in beam flanges [9]. The study conducted by Jones et al. [10] also confirmed that RBS moment connections with relatively strong panel zones result in enhanced performance. In another study, Tahamouli Roudsari et al. [11] compared the seismic performances of shallow beam connections with accordion webs and reduced sections. Their results showed that samples with RBS connections exhibited higher ductility, better energy dissipation, and hence a superior seismic performance compared to the samples with only corrugated beam webs.

The influence that vertical loads can have on the working mechanism of RBS connections is either neglected or not adequately accounted for in many of the research projects and experiments involving such connections. To address this issue, Montuori's study [12] investigated the effect of gravity loads on the design of RBS connections by presenting a new procedure for accurately determining the relationship among RBS location, vertical load, and the amount of section reduction to ensure the proper development of plastic hinges in the beam. The abovementioned study provides a design abacus that can be efficiently utilized to determine the best RBS location for optimum seismic performance.

Cutting the beam flange, especially in narrow sections such as IPE profiles, results in an increased potential for the web local buckling, beam lateral-torsional buckling, and decreased beam strength. The study by Tahamouli Roudsari et al. [13] presented a simple method to improve the efficiency of IPE beams with radius-cut reduced sections by using horizontal and vertical stiffeners for the beam web. Their results revealed that the simultaneous application of horizontal and vertical stiffeners of the beam web largely prevented the decline of the corresponding hysteresis loops and improved the behavior of the connection. Hence, they recommended utilizing such modified RBS connections in areas with high relative seismic risk. In another paper, Moradi Garoosi et al. [14] investigated the idea of rigid connections with replaceable RBS fuses that could be easily repaired after major earthquakes. They concluded that such connections decrease the damage inflicted on the column and the panel zone and provide very good ductility, making them a suitable alternative to the conventional RBS connections. Montuori and Sagarese's study [15] also proposed utilizing steel RBS to improve the ductility of wooden frames. The presented design helps protect beam-to-column connections and the intermediate sections of the wooden beams as horizontal forces increase during seismic activity. The study considers the roles of vertical loads and the amount of section

reduction in the mechanism of the RBS connection and provides a series of easy-to-use design charts.

In 2017, Morshedi et al. [16] introduced a new beam-to-column connection for steel moment frames termed the double reduced beam section (DRBS) connection to delay buckling failure modes and achieve a more ductile seismic behavior. This design adds an extra reduced section to the prequalified radius-cut RBS connection and aims to shift the plastic hinge further away from the beam-column interface. The seismic performance of this connection was evaluated through finite element modeling. The results showed that the DRBS connection has excellent hysteresis behavior. Also, the DRBS connection resulted in up to 40% more deformation capacity than the RBS connection. Plasticization of both reduced beam sections delayed the failure buckling modes and resulted in a 50–75% increase in the seismic energy absorbed prior to buckling, compared to the RBS connection. Furthermore, the addition of a second reduced section distributed the strains over the two reduced sections, which led to a 35–60% decrease in the equivalent plastic strain at the reduced sections, at the 6% story drift [16].

In 2019, Sai Chandana et al. [17] conducted a numerical study on RBS and DRBS connections. Their results suggest that these connections can withstand large inelastic strains and limit the stress concentration in the connection.

The abovementioned simultaneous plasticization of the two reduced sections in the DRBS connection leading to an extended plastic hinge can be achieved by keeping the bending moment demand-capacity ratio (DCR) equal in the middle of these reduced sections. To do so, the depth of the two cuts in the DRBS connection (c_1 and c_2 values) must be determined according to the bending moment diagram in the beam. Based on such a design criterion, considering that the bending moment decreases with distance from the column face, selecting a greater depth for the second cut ($c_2 > c_1$) enables the two reduced sections to act as a dual fuse through simultaneous plasticization.

In general, in first-order analyses, obtaining the elastic displacement of the structure is an easy and routine practice. Factors such as nonlinear effects can be taken into account by multiplying a coefficient by the obtained displacement value [18]. Several studies have been carried out to provide a simple and accurate method for understanding the effect of utilizing reduced beam section connections on the stiffness of steel moment frames. In 2003, Chambers et al. [19] derived the closed-form stiffness matrix of a two-dimensional steel moment frame with radius-cut RBS connections based on the principle of virtual work. Their results indicated decreases in stiffness terms varying between 3.6% to 15.1% and a 10.4% decrease in rotational stiffness. They also found that relationships between the stiffness terms and the reduced flange width are nonlinear. Chambers et al. [19] also conducted parametric studies on six-story, two- and three-span steel moment frames subjected to seismic base shears and compared the elastic drift coefficients calculated for frames with and without RBS connections. The greatest amount of flange cross-section reduction considered in their study was a maximum 40% flange width reduction in all the beam flanges. Compared to the frames without RBS connections, the considered flange reductions resulted in 10.6% and 10.3% increases in the story drift of the two-span and three-span frames, respectively [19]. In 2006, Lee and Chung [20] introduced a simplified analytical method for estimating the lateral displacement of steel moment frames with radius-cut RBS connections. Because of the geometry of the radius-cut RBS connection, the mathematical formula based on the conjugate beam method becomes complicated when it is used to calculate the component of the story drift contributed by the beam. In the study mentioned above, this issue was circumvented by substituting the considered RBS connection with an equivalent beam with constant width. The equivalence between the two beams was established by considering an equal flange elongation criterion in the RBS region [20].

FEMA 350 [21] recommends that instead of specific calculations, a 9% increase be considered for reductions in beam flange width up to 50% and that interpolation be used for lesser beam flange reduction percentages. Nevertheless, the basis for this simplification is not provided in this document or other sources, and the recommended approach does not give an accurate estimate [19].

ANSI/AISC 358-16 [22] also recommends that instead of more detailed calculations, the effective elastic drift be calculated by multiplying the elastic frame drift based on gross beam sections by 1.1 for reductions in beam flange width up to 50% and that interpolation be used for lesser beam flange reduction percentages.

In 2019, Fanaie et al. [18] presented an improved and innovative approach for calculating the amplified elastic story drift in steel moment frames induced by RBS connections. Studies conducted before this research involved complicated mathematical formulae and did not consider all shear, axial, and flexural deformations in the moment frames. Hence, they did not provide accurate estimations of the stiffness variation. To address these issues, Fanaie et al. [18], considering all lateral deformations in a single-story single-span steel moment frame with RBS connections, developed a practical and straightforward formulation for calculating the elastic drift amplification factor. Using the method of virtual work, they first provided an exact calculation of the elastic drift in a frame with radius-cut RBS connections. Then, by performing sensitivity analysis, they determined the connection parameters with the most significant effect on the calculated elastic drift. Based on these parameters and employing the response surface method (RSM), separate and simplified elastic drift amplification factor formulae were presented for IPE and HEA beam profiles [18].

Since the DRBS connection has been shown to improve the seismic behavior of the RBS connection in the studies conducted, it is expected to be soon utilized in the construction industry. Nevertheless, considering that the most important disadvantage of moment frames is their low lateral stiffness, using two reduced sections instead of one near the beam-to-column connections in such frames intensifies this problem. Drift control should thus be regarded as a serious concern in moment resisting frames incorporating DRBS connections. Therefore, there appears to be a need for an accurate yet simple method to examine the stiffness variation in steel moment frames due to the utilization of DRBS connections.

The objective of this research was to investigate the effect of the DRBS connections on the stiffness of steel moment frames through presenting a theoretical approach based on mathematical relationships and structural analysis principles. For this purpose, similar to the work done by Fanaie et al. [18], first, based on geometric relationships and utilizing the method of virtual work, the exact formulae for calculating the elastic drift and the elastic drift amplification factor in a steel moment frame with DRBS connections, without considering any specific sections for beams and columns, were developed. Next, by carrying out a sensitivity analysis, the most effective DRBS connection parameters on the elastic drift of the studied moment frame were identified. The accuracy of the developed exact theoretical formulae and the performed sensitivity analysis was then confirmed through finite element modeling of the considered frame. In the next step, the RSM was utilized to derive highly accurate and specific relationships for the elastic drift amplification factor in moment frames with DRBS connections made of the different HEA and IPE sections considered. Ultimately, using the envelope curves of the derived relationships, two accurate and simple formulae based on DRBS connection parameters were proposed for estimating the elastic drift amplification factor in steel moment frames with DRBS connections constructed of HEA and IPE sections.

2. Calculation of the exact elastic drift amplification factor in a single-story single-span steel moment frame with DRBS connections

In this section, the exact amount of the elastic drift in a single-story single-span steel moment frame with rigid DRBS beam-to-column connections subjected to the horizontal force P is investigated. It should be noted that in the procedure presented in the following, the type of I-

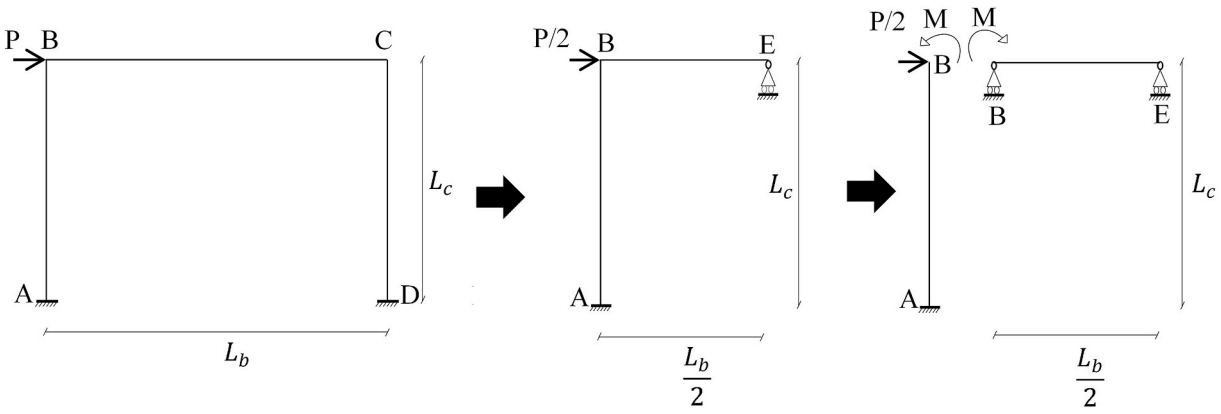

Fig. 2. Conversion of the considered two-dimensional frame into a half-frame.

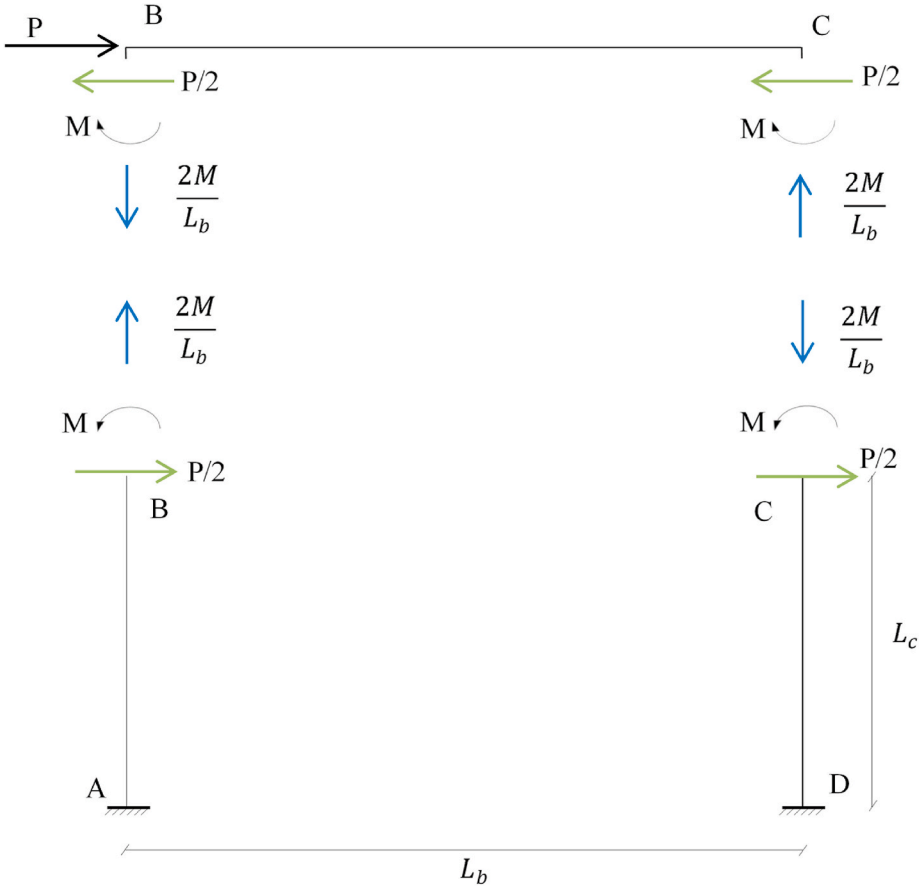

Fig. 3. Analysis of the forces in the steel moment frame subjected to the lateral force *P*.

shaped steel section is not of importance, and the only assumption governing the relationships is that the sections used for beams and columns are the same. Fig. 2 shows the schematic view of the two-dimensional frame considered.

First, according to the geometry of the frame and the loading applied, the structural analysis rules applicable to symmetrical structures subjected to antisymmetric loading is used to convert the considered moment frame into a half-frame (Fig. 2). In the next step, the resulting half-frame is examined using the analytical method of virtual work.

If the DRBS connections are neglected, the amount of internal bending moment (M) could be calculated using the compatibility equation for the equality of the rotations on the two sides of node B as follows:

$$\theta_{B_L}=\theta_{B_R}\rightarrow\frac{\frac{P}{2}\cdot L_c^2}{2EI_c}-\frac{ML_c}{EI_c}=\frac{M\cdot\frac{L_b}{2}}{3EI_b}$$
$$\rightarrow\frac{M}{6E}\left(\frac{6L_c}{I_c}+\frac{L_b}{I_b}\right)=\frac{PL_c^2}{4EI_c}\rightarrow M=\frac{\frac{1.5PL_c^2}{I_c}}{\frac{6L_c}{I_c}+\frac{L_b}{I_b}} \quad (1)$$

In Eq. (1), L_c and L_b are the column length and beam length

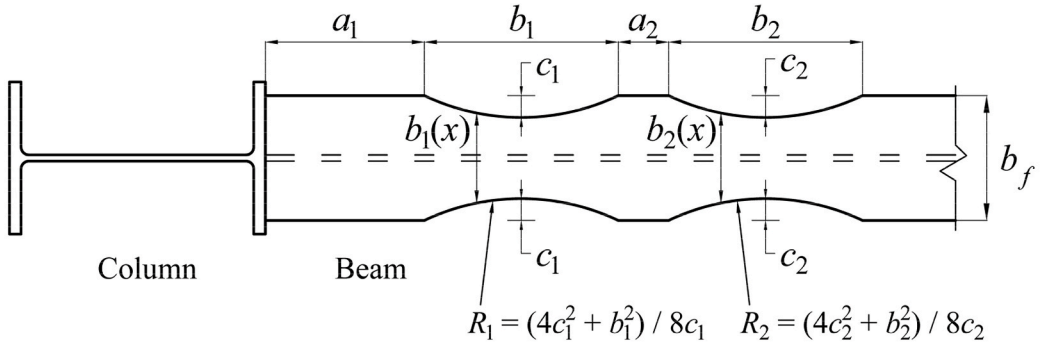

(a)

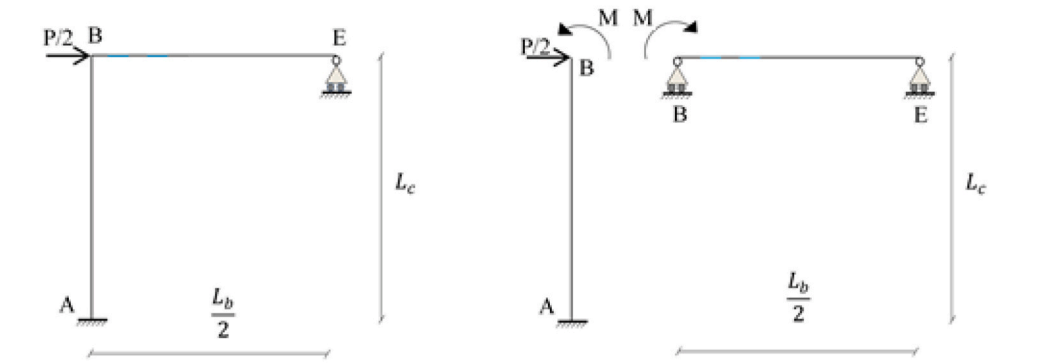

(b)

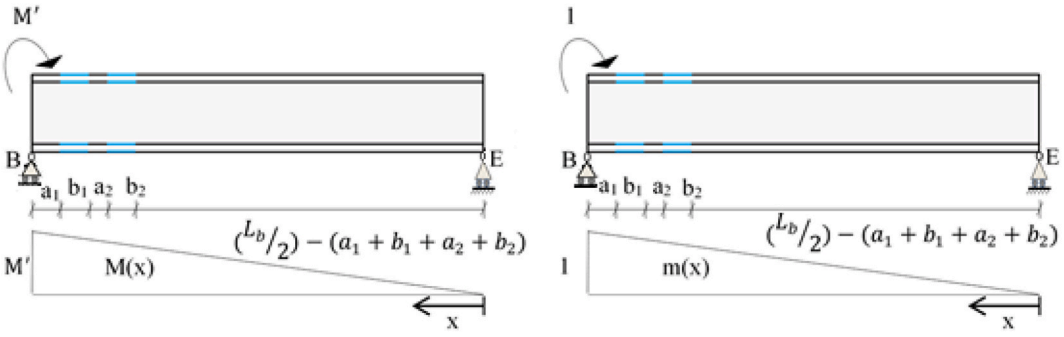

(c)

Fig. 4. (a) The DRBS connection; (b) The resulting half-frame obtained by splitting the considered moment frame based on its symmetrical geometry; (c) Moment diagrams of the half-frame in analysis using the method of virtual work.

(distances between the centerlines), respectively, and E is the modulus of elasticity of the steel used. Besides, I_c and I_b denote the moments of inertia of the beam and column sections, respectively, and M is the internal bending moment in node B in the case where DRBS connections are neglected.

According to the moment obtained from Eq. (1), the amount of elastic drift of the frame without considering the DRBS connections and only caused by the flexural deformations is calculated using Eq. (2):

$$\Delta_{Bending} = \frac{PL_c^3}{6EI_c} - \frac{ML_c^2}{2EI_c} \tag{2}$$

According to the analysis of the forces in the moment frame under study, presented in Fig. 3, since the beam and column sections selected are the same, the amounts of elastic drift caused by shear and axial deformations in the frame members are respectively calculated from Eqs. (3) and (4) as follows:

$$\begin{aligned}\Delta_{Shear} &= \int \frac{V(x)v(x)}{GA_s}dx = \sum \frac{VvL}{GA_s} \\ &= 2\frac{\frac{P}{2}\cdot\frac{1}{2}\cdot L_c}{GA_s} + \frac{\frac{2M}{L_b}\cdot\frac{2M}{PL_b}\cdot L_b}{GA_s} = \frac{\frac{PL_c}{2} + \frac{4M^2}{PL_b}}{GA_s}\end{aligned} \tag{3}$$

$$\begin{aligned}\Delta_{Axial} &= \int \frac{N(x)n(x)}{AE}dx = \sum \frac{NnL}{AE} \\ &= 2\frac{\frac{2M}{L_b}\cdot\frac{2M}{PL_b}\cdot L_c}{A_cE} = \frac{8M^2L_c}{PL_b^2A_cE}\end{aligned} \tag{4}$$

In the above equations, $G = E/2(1+\nu)$ and $\nu = 0.3$ are respectively

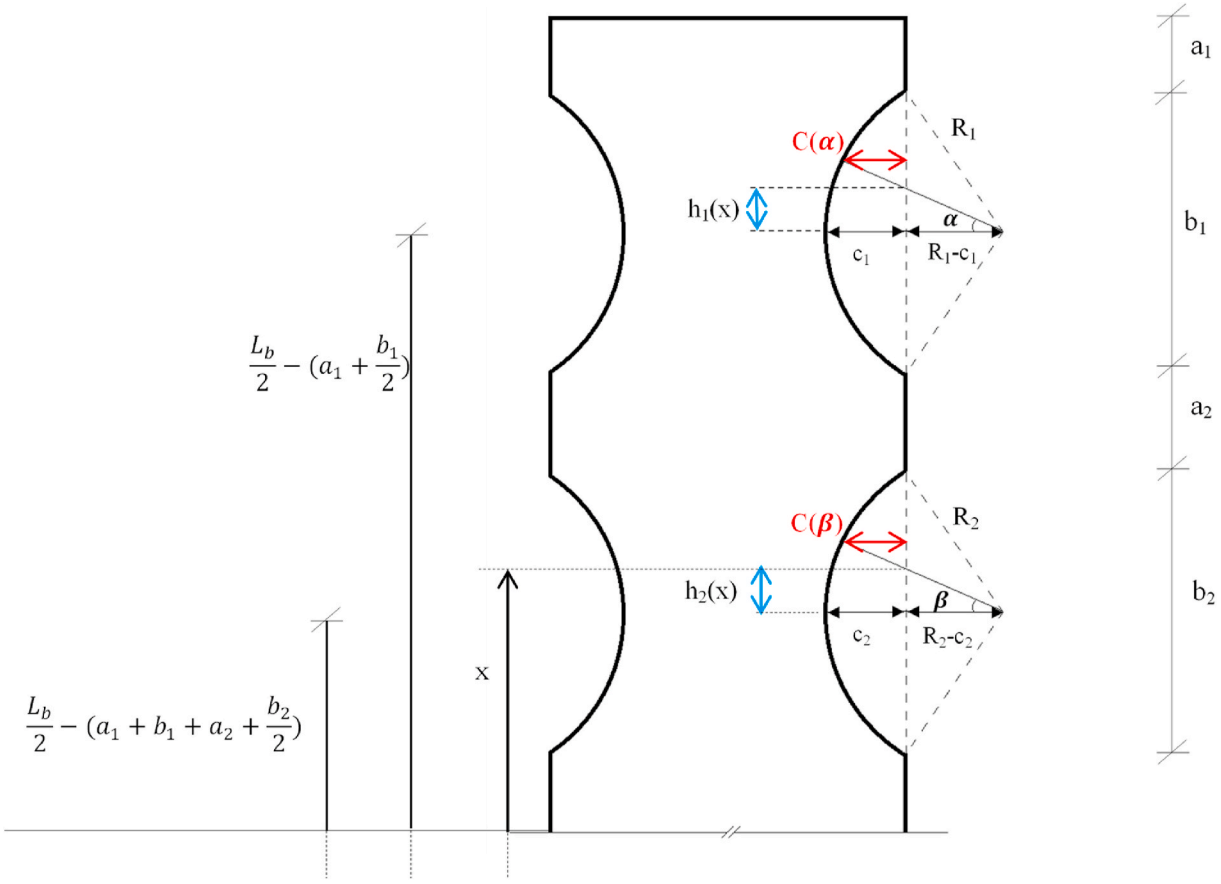

Fig. 5. The geometrical parameters in the DRBS connection.

the shear modulus and Poisson's ratio of the steel used. Also, A_c denotes the cross-sectional area of the columns in the frame and A_s denotes the effective shear cross-sectional area of the beams and columns in the frame, which for I-shaped sections, is equal to the area of the cross-sectional area of the web ($h_w.t_w$). By adding up Eqs. (1)–(3), the total amount of elastic drift of the steel moment frame subjected to the lateral force P, without considering the DRBS connections, is calculated as follows:

$$\begin{aligned}\Delta_{Total} &= \Delta_{Bending} + \Delta_{Shear} + \Delta_{Axial} \\ &= \frac{PL_c^3}{6EI_c} - \frac{ML_c^2}{2EI_c} + \frac{P^2L_cL_b + 8M^2}{2PL_bGA_s} + \frac{8M^2L_c}{PL_b^2A_cE}\end{aligned} \tag{5}$$

By considering the connections in the moment frame as DRBS connections with specifications shown in Fig. 4 (a), the amount of rotation on the right side of node B becomes greater than that calculated by Eq. (1). Therefore, as depicted in Fig. 4 (b) and 4 (c), by using the method of virtual work and applying a unit moment to node B, the amount of rotation on the right side of node B while utilizing DRBS connections could be calculated based on the equality of the internal and external work done in the half-beam using Eq. (6):

$$\begin{aligned}1 \times \theta'_{B_R} &= \int_0^{\frac{L_b}{2}} \frac{M'(x)m'(x)}{EI(x)}dx \\ &= \int_0^{\frac{L_b}{2}} \frac{2M'x}{\frac{L_b}{2}} \frac{2x}{\frac{L_b}{2}} dx = \frac{4M'}{EL_b^2}\int_0^{\frac{L_b}{2}} \frac{x^2}{I(x)}dx\end{aligned} \tag{6}$$

where M' is the internal bending moment in node B while utilizing DRBS connections in the frame.

Considering the location and geometry of the DRBS connection in the half-beam, the integral in Eq. (6) is rewritten as follows:

$$\theta'_{B_R} = \theta'_1 + \theta'_2 + \theta'_3 + \theta'_4 + \theta'_5 \tag{7}$$

According to the integration limits for each part of the beam, we have:

$$\theta'_1 = \frac{4M'}{EL_b^2I_b}\int_0^{\frac{L_b}{2}-(a_1+b_1+a_2+b_2)} x^2dx \tag{8}$$

$$\theta'_2 = \frac{4M'}{EL_b^2}\int_{\frac{L_b}{2}-(a_1+b_1+a_2)}^{\frac{L_b}{2}-(a_1+b_1+a_2+b_2)} \frac{x^2}{I_2(x)}dx \tag{9}$$

$$\theta'_3 = \frac{4M'}{EL_b^2I_b}\int_{\frac{L_b}{2}-(a_1+b_1+a_2)}^{\frac{L_b}{2}-(a_1+b_1)} x^2dx \tag{10}$$

$$\theta'_4 = \frac{4M'}{EL_b^2}\int_{\frac{L_b}{2}-(a_1+b_1)}^{\frac{L_b}{2}-(a_1)} \frac{x^2}{I_1(x)}dx \tag{11}$$

$$\theta'_5 = \frac{4M'}{EL_b^2I_b}\int_{\frac{L_b}{2}-(a_1)}^{\frac{L_b}{2}} x^2dx \tag{12}$$

For cross-sections not located within the range of the radius-cut reduced sections in the flanges, the calculation of the second moment of area is a simple task and could be done using the following equation:

$$I_b = \frac{1}{12}\left[b_f\left(h_w + 2t_f\right)^3 - \left(b_f - t_w\right)h_w^3\right] \tag{13}$$

Nevertheless, the calculation of the second moment of the area for

the cross-sections located within the radius-cut reduced sections, due to the variable cross-section of the flanges, poses the main challenge in the calculations related to the steel moment frames with DRBS connections. According to Fig. 5, in the cross-sections located at the distance x from node E, where x belongs to the interval extended from the start to the end of the first reduced section, the flange width is as follows:

$$b_1(x) = b_f + 2R_1 - 2c_1 - 2\sqrt{R_1^2 - \left(x - \left(\frac{L_b}{2} - a_1 - \frac{b_1}{2}\right)\right)^2} \tag{14}$$

Therefore, the second moment of area for such cross-sections could be calculated as follows:

$$I_1(x) = \frac{1}{12}\left[b_1(x)\left(h_w+2t_f\right)^3 - (b_1(x)-t_w)h_w^3\right] = \frac{1}{12}\left[\begin{array}{l}\left(b_f+2R_1-2c_1-2\sqrt{R_1^2-\left(x-\left(\frac{L_b}{2}-\left(a_1+\frac{b_1}{2}\right)\right)\right)^2}\right)\\ \cdot\left[\left(h_w+2t_f\right)^3-h_w^3\right]+t_w h_w^3\end{array}\right] \tag{15}$$

Also, according to Fig. 5, in the cross-sections located at the distance x from Node E, where x belongs to the interval extended from the start to the end of the second reduced section, the flange width could be obtained using the following equation:

$$b_2(x) = b_f + 2R_2 - 2c_2 - 2\sqrt{R_2^2 - \left(x - \left(\frac{L_b}{2} - \left(a_1 + b_1 + a_2 + \frac{b_2}{2}\right)\right)\right)^2} \tag{16}$$

Hence, the second moment of area for such cross-sections is given by the following equation:

$$I_2(x) = \frac{1}{12}\left[b_2(x)\left(h_w+2t_f\right)^3 - (b_2(x)-t_w)h_w^3\right] = \frac{1}{12}\left[\begin{array}{l}\left(b_f+2R_2-2c_2-2\sqrt{R_2^2-\left(x-\left(\frac{L_b}{2}-\left(a_1+b_1+a_2+\frac{b_2}{2}\right)\right)\right)^2}\right)\\ \cdot\left[\left(h_w+2t_f\right)^3-h_w^3\right]+t_w h_w^3\end{array}\right] \tag{17}$$

The DRBS connection parameters (a_1, a_2, b_1, b_2c_1, c_2 R_1, R_2,) and the I-shaped beam specifications (b_f, h_wt_f, and t_w) are shown in Fig. 4 (a). According to Eqs. (8)–(12) and (15) and (17), the terms on the right side of Eq. (7) could be rewritten as in the following:

In the interval $0 \le x \le \frac{L_b}{2} - (a_1 + b_1 + a_2 + b_2)$, the flange width has a constant value and is equal to b_f. Hence, for $\theta_1^{'}$ we have:

$$\theta^{'}{}_1 = \frac{4M^{'}}{\frac{1}{12}\left[b_f\left(h_w+2t_f\right)^3-\left(b_f-t_w\right)h_w^3\right]EL_b^2}\cdot\frac{\left(\frac{L_b}{2}-(a_1+b_1+a_2+b_2)\right)^3}{3} \tag{18}$$

In the interval $\frac{L_b}{2} - (a_1 + b_1 + a_2 + b_2) \le x \le \frac{L_b}{2} - (a_1 + b_1 + a_2)$, the flange width has a variable value, and hence Eq. (17) must be used for calculating the second moment of the area. Therefore, for $\theta_2^{'}$ we have:

$$\theta^{'}{}_2 = \frac{4M^{'}}{EL_b^2}\int_{\frac{L_b}{2}-(a_1+b_1+a_2+b_2)}^{\frac{L_b}{2}-(a_1+b_1+a_2)} \frac{x^2dx}{\frac{1}{12}\left[\begin{array}{l}\left(b_f+2R_2-2c_2-2\sqrt{R_2^2-\left(x-\left(\frac{L_b}{2}-\left(a_1+b_1+a_2+\frac{b_2}{2}\right)\right)\right)^2}\right)\\ \cdot\left[\left(h_w+2t_f\right)^3-h_w^3\right]+t_w h_w^3\end{array}\right]} \tag{19}$$

The calculation process of $\theta_3^{'}$ is similar to that of $\theta_1^{'}$ except that the corresponding interval is $\frac{L_b}{2} - (a_1 + b_1 + a_2) \le x \le \frac{L_b}{2} - (a_1 + b_1)$. Hence, we have:

$$\theta'_3 = \frac{4M'}{\frac{1}{12}\left[b_f(h_w+2t_f)^3-(b_f-t_w)h_w^3\right]EL_b^2}\cdot\frac{\left(\frac{L_b}{2}-(a_1+b_1)\right)^3-\left(\frac{L_b}{2}-(a_1+b_1+a_2)\right)^3}{3} \quad (20)$$

In the interval $\frac{L_b}{2}-(a_1+b_1)\le x\le\frac{L_b}{2}-(a_1)$, the flange width also has a variable value, and hence Eq. (15) must be used to calculate the second moment of area. Thus, for θ'_4 we have:

$$\theta'_4=\frac{4M'}{EL_b^2}\int_{\frac{L_b}{2}-a_1-b_1}^{\frac{L_b}{2}-a_1}\frac{x^2}{\frac{1}{12}\left[\begin{pmatrix} b_f+2R_1-2c_1 \\ -2\sqrt{R_1^2-\left(x-\left(\frac{L_b}{2}-\left(a_1+\frac{b_1}{2}\right)\right)\right)^2}\end{pmatrix}\cdot\left[(h_w+2t_f)^3-h_w^3\right]+t_wh_w^3\right]}dx \quad (21)$$

In the interval $\frac{L_b}{2}-a_1\le x\le\frac{L_b}{2}$, the flange width has a constant value and is equal to b_f. Therefore, for θ'_5 we have:

$$\theta'_5 = \frac{4M'}{\frac{1}{12}\left[b_f(h_w+2t_f)^3-(b_f-t_w)h_w^3\right]EL_b^2}\cdot\frac{\left(\frac{L_b}{2}\right)^3-\left(\frac{L_b}{2}-a_1\right)^3}{3} \quad (22)$$

According to Fig. 5, the value of the parameter $c(\alpha)$ along the first radius-cut reduced section in the beam flange could be calculated as follows:

$$\begin{aligned} c(\alpha) &= R_1\cos\alpha-(R_1-c_1)=\left(\frac{b_1^2+4c_1^2}{8c_1}\right)cos\alpha-\left(\frac{b_1^2+4c_1^2}{8c_1}-c_1\right) \\ &=\left(\frac{b_1^2+4c_1^2}{8c_1}\right)\cos\alpha-\left(\frac{b_1^2-4c_1^2}{8c_1}\right) \end{aligned} \quad (23)$$

Based on Eq. (23) and Fig. 5, the variable flange width along the first reduced section ($b_1(x)$) could be redefined as $b_1(x) = b_f-2c_1(x)$. Hence, the following equation could be written:

$$b_1(\alpha) = b_f-2c_1(\alpha) = b_f-\left(\frac{b_1^2+4c_1^2}{4c_1}\right)\cdot cos\,\alpha+\left(\frac{b_1^2-4c_1^2}{4c_1}\right) \quad (24)$$

According to Fig. 5, $\cos\alpha$ could be defined as a function of x as follows:

$$h_1(x)=x-\left(\frac{L_b}{2}-a_1-\frac{b_1}{2}\right)=x+a_1+\frac{b_1}{2}-\frac{L_b}{2} \quad (25)$$

where $\frac{L_b}{2}-a_1\le x\le\frac{L_b}{2}-a_1-b_1$.

According to Eq. (25) obtained for $h_1(x)$, $\tan\alpha$ is rewritten as in the following:

$$\begin{aligned} \tan\alpha &=\frac{h_1(x)}{R_1-c_1}=\frac{x+a_1+\frac{b_1}{2}-\frac{L_b}{2}}{\frac{b_1^2+4c_1^2}{8c_1}-c_1}=\frac{x+a_1+\frac{b_1}{2}-\frac{L_b}{2}}{\frac{b_1^2-4c_1^2}{8c_1}} \\ &=\frac{8c_1\left(x+a_1+\frac{b_1}{2}-\frac{L_b}{2}\right)}{\left(b_1^2-4c_1^2\right)}=\frac{8c_1\left(x+a_1+\frac{b_1}{2}-\frac{L_b}{2}\right)}{(b_1-2c_1)(b_1+2c_1)} \end{aligned} \quad (26)$$

Considering that $\cos\alpha=1/\sqrt{1+\tan\alpha^2}$ and based on Eq. (26) obtained for $\tan\alpha$, $\cos\alpha$ could be calculated as follows:

$$\begin{aligned} \cos\alpha &=\frac{1}{\sqrt{1+\tan\alpha^2}}=\frac{1}{\sqrt{1+\frac{64c_1^2\left(x+a_1+\frac{b_1}{2}-\frac{L_b}{2}\right)^2}{(b_1+2c_1)^2(b_1-2c_1)^2}}}=\frac{1}{\sqrt{\frac{(b_1+2c_1)^2(b_1-2c_1)^2+64c_1^2\left(x+a_1+\frac{b_1}{2}-\frac{L_b}{2}\right)^2}{(b_1+2c_1)^2(b_1-2c_1)^2}}} \\ &=\frac{(b_1+2c_1)(b_1-2c_1)}{\sqrt{(b_1+2c_1)^2(b_1-2c_1)^2+64c_1^2\left(x+a_1+\frac{b_1}{2}-\frac{L_b}{2}\right)^2}} \end{aligned} \quad (27)$$

Table 1
The specifications of the selected beam and column sections.

Section	H (mm)	t_w (mm)	b_f (mm)	t_f (mm)	A_c (cm^2)	A_s (cm^2)	I (cm^4)
HEA500	490	12.0	300	23.0	198.0	53.28	86970
HEA1000	990	16.5	300	31.0	347.0	153.12	553800
IPE300	300	7.1	150	10.7	53.8	19.78	8360
IPE600	600	12.0	220	19.0	156.0	67.44	92080

Table 2
Characteristics of the steel used in the moment frame.

E (MPa)	ν
200,000	0.3

Since $\tan\alpha$ is raised to the power of 2 in Eq. (27), the effects of its value being negative along half of the first reduced section are eliminated. By substituting $\cos\alpha$ in Eq. (24), $b_1(\alpha)$ is written as in the following:

$$b_1(\alpha) = b_f - \left(\frac{b_1^2+4c_1^2}{4c_1}\right)\frac{(b_1+2c_1)(b_1-2c_1)}{\sqrt{(b_1+2c_1)^2(b_1-2c_1)^2+64c_1^2\left(x+a_1+\frac{b_1}{2}-\frac{L_b}{2}\right)^2}} + \left(\frac{b_1^2-4c_1^2}{4c_1}\right) \tag{28}$$

Ultimately, based on Eqs. (11), (15) and (28), the value of $\theta_4^{'}$ could be calculated using Eq. (29) as follows:

$$\begin{aligned}\theta_4^{'} &= \frac{4M^{'}}{EL_b^2}\int_{\frac{L_b}{2}-a_1-b_1}^{\frac{L_b}{2}-a_1}\frac{x^2dx}{\frac{1}{12}\left[b_1(x)\left\{(h_w+2t_f)^3-h_w^3\right\}+t_wh_w^3\right]}\\ &= \frac{4M^{'}}{EL_b^2}\int_{\frac{L_b}{2}-a_1-b_1}^{\frac{L_b}{2}-a_1}\frac{x^2dx}{\frac{1}{12}\left[\left(b_f-\left(\frac{b_1^2+4c_1^2}{4c_1}\right)\cdot\frac{(b_1+2c_1)(b_1-2c_1)}{\sqrt{(b_1+2c_1)^2(b_1-2c_1)^2+64c_1^2\left(x+a_1+\frac{b_1}{2}-\frac{L_b}{2}\right)^2}}+\left(\frac{b_1^2-4c_1^2}{4c_1}\right)\right)\cdot\left\{(h_w+2t_f)^3-h_w^3\right\}+t_wh_w^3\right]}\end{aligned} \tag{29}$$

According to Fig. 5, in a similar manner as the above calculations, the value of the parameter $c(\beta)$ along the second radius-cut reduced section in the beam flange could be calculated as follows:

$$\begin{aligned}c(\beta) &= R_2\cdot\cos\beta-(R_2-c_2) = \left(\frac{b_2^2+4c_2^2}{8c_2}\right)\cdot cos\,\beta-\left(\frac{b_2^2+4c_2^2}{8c_2}-c_2\right)\\ &= \left(\frac{b_2^2+4c_2^2}{8c_2}\right)\cdot cos\,\beta-\left(\frac{b_2^2-4c_2^2}{8c_2}\right)\end{aligned} \tag{30}$$

The variable flange width along the second reduced section ($b_2(x)$) is redefined using Eq. (30) as $b_2(x) = b_f - 2c_2(x)$. Hence, the following equation could be written:

$$b_2(\beta) = b_f - 2c_2(\beta) = b_f - \left(\frac{b_2^2+4c_2^2}{4c_2}\right)\cdot cos\,\beta + \left(\frac{b_2^2-4c_2^2}{4c_2}\right) \tag{31}$$

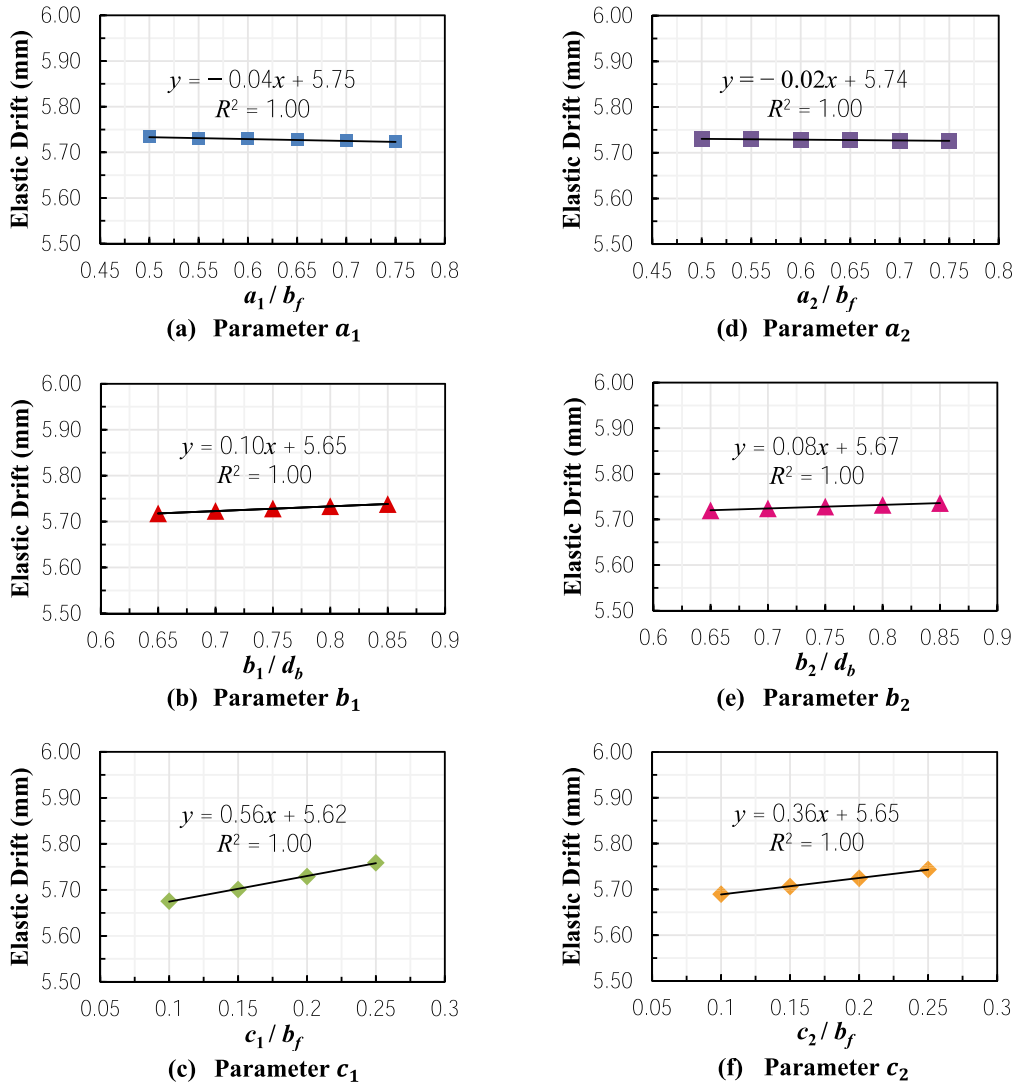

Fig. 6. Results of the sensitivity analysis of the DRBS connection parameters while using the HEA500 section: (a) Parameter a_1; (b) Parameter b_1; (c) Parameter c_1; (d) Parameter a_2; (e) Parameter b_2; (f) Parameter c_2.

Based on Fig. 5, $\cos\beta$ could be defined as a function of x as in the following:

$$\begin{aligned} h_2(x) &= x-\left(\frac{L_b}{2}-a_1-b_1-a_2-\frac{b_2}{2}\right) \\ &= x+a_1+b_1+a_2+\frac{b_2}{2}-\frac{L_b}{2} \end{aligned} \tag{32}$$

where $\frac{L_b}{2}-a_1-b_1-a_2-b_2 \le x \le \frac{L_b}{2}-a_1-b_1-a_2$.

According to Eq. (32) obtained for $h_2(x)$, $\tan\beta$ is rewritten as follows:

$$\begin{aligned} \tan\beta &= \frac{h_2(x)}{R_2-c_2}=\frac{x+a_1+b_1+a_2+\frac{b_2}{2}-\frac{L_b}{2}}{\frac{b_2^2+4c_2^2}{8c_2}-c_2}=\frac{x+a_1+b_1+a_2+\frac{b_2}{2}-\frac{L_b}{2}}{\frac{b_2^2-4c_2^2}{8c_2}} \\ &=\frac{8c_2\left(x+a_1+b_1+a_2+\frac{b_2}{2}-\frac{L_b}{2}\right)}{\left(b_2^2-4c_2^2\right)}=\frac{8c_2\left(x+a_1+b_1+a_2+\frac{b_2}{2}-\frac{L_b}{2}\right)}{(b_2-2c_2)(b_2+2c_2)} \end{aligned} \tag{33}$$

Considering that $\cos\beta=1/\sqrt{1+\tan\beta^2}$ and based on Eq. (33) obtained for $\tan\beta$, $\cos\beta$ could be calculated as follows:

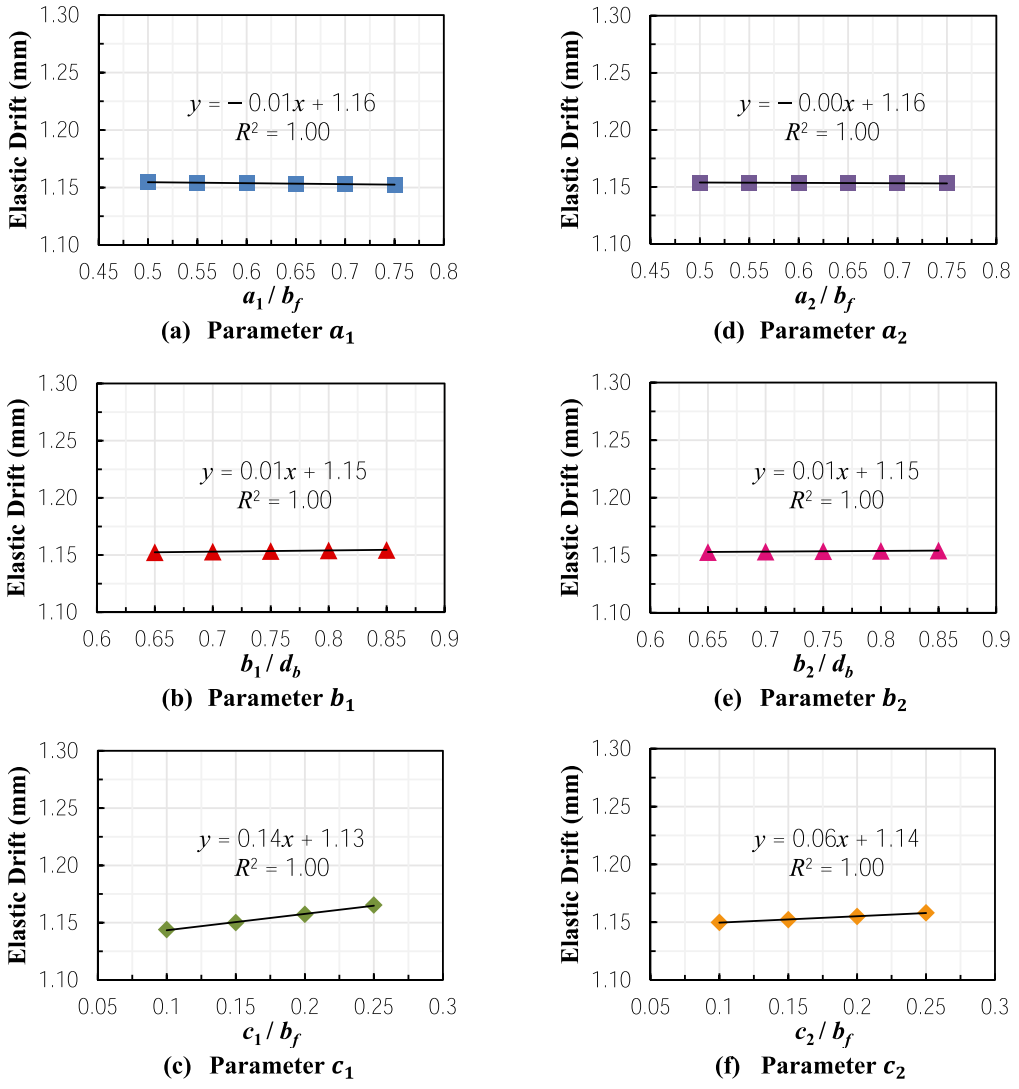

Fig. 7. Results of the sensitivity analysis of the DRBS connection parameters while using the HEA1000 section: (a) Parameter a_1; (b) Parameter b_1; (c) Parameter c_1; (d) Parameter a_2; (e) Parameter b_2; (f) Parameter c_2.

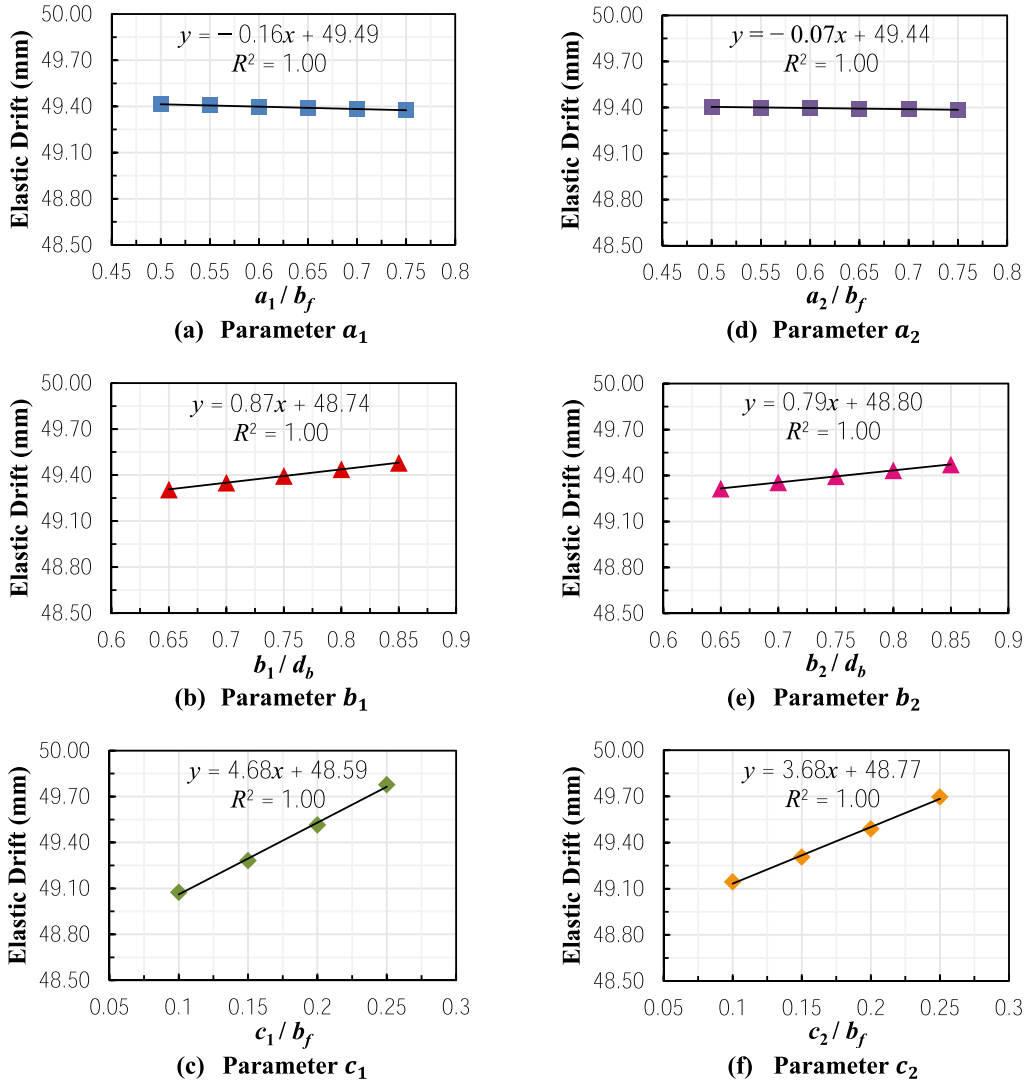

Fig. 8. Results of the sensitivity analysis of the DRBS connection parameters while using the IPE300 section: (a) Parameter a_1; (b) Parameter b_1; (c) Parameter c_1; (d) Parameter a_2; (e) Parameter b_2; (f) Parameter c_2.

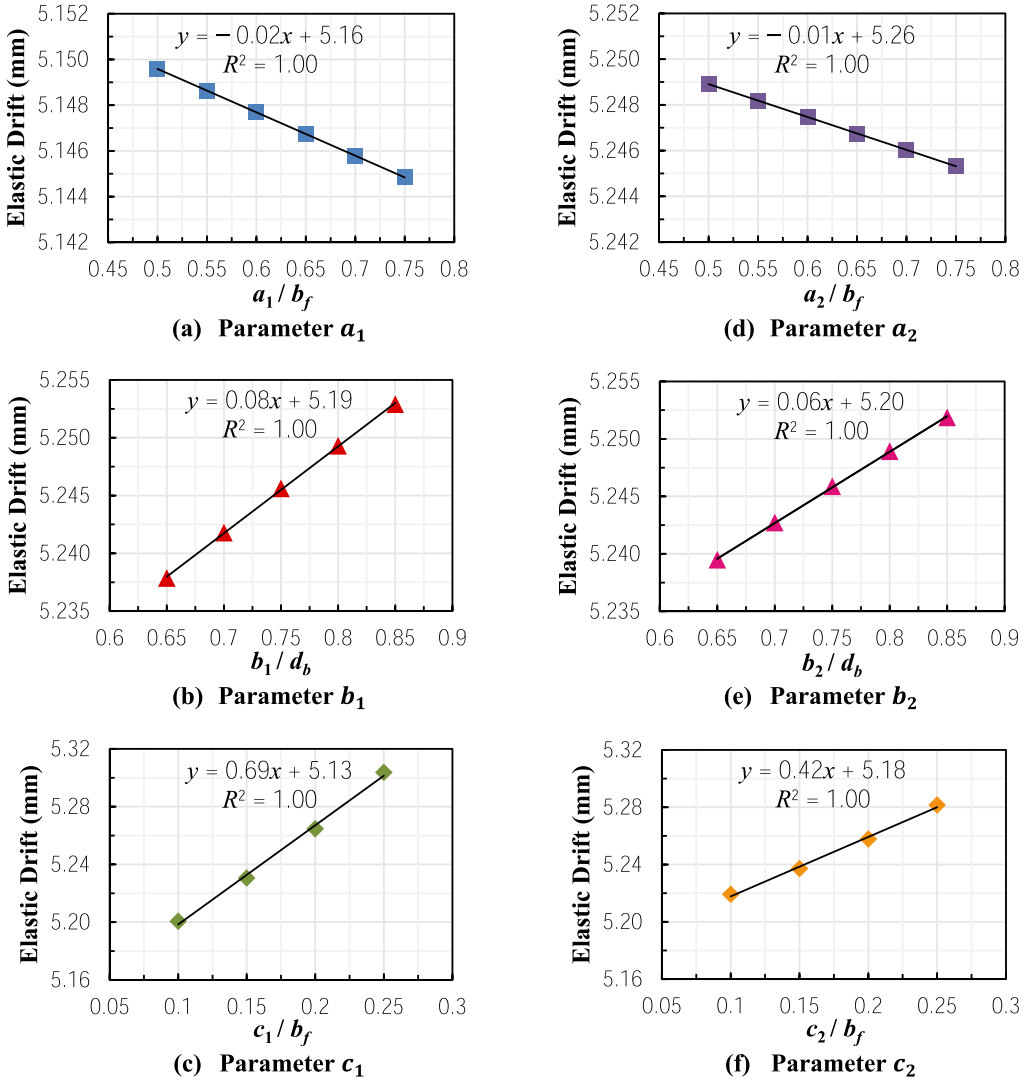

Fig. 9. Results of the sensitivity analysis of the DRBS connection parameters while using the IPE600 section: (a) Parameter a_1; (b) Parameter b_1; (c) Parameter c_1; (d) Parameter a_2; (e) Parameter b_2; (f) Parameter c_2.

$$\cos\beta = \frac{1}{\sqrt{1+\tan\beta^2}} = \frac{1}{\sqrt{1+\dfrac{64c_2^2\left(x+a_1+b_1+a_2+\dfrac{b_2}{2}-\dfrac{L_b}{2}\right)^2}{(b_2-2c_2)^2(b_2+2c_2)^2}}}$$
$$= \frac{1}{\sqrt{\dfrac{(b_2-2c_2)^2(b_2+2c_2)^2+64c_2^2\left(x+a_1+b_1+a_2+\dfrac{b_2}{2}-\dfrac{L_b}{2}\right)^2}{(b_2-2c_2)^2(b_2+2c_2)^2}}}$$
$$= \frac{(b_2+2c_2)(b_2-2c_2)}{\sqrt{(b_2-2c_2)^2(b_2+2c_2)^2+64c_2^2\left(x+a_1+b_1+a_2+\dfrac{b_2}{2}-\dfrac{L_b}{2}\right)^2}} \tag{34}$$

Since $\tan\beta$ is raised to the power of 2 in Eq. (34), the effects of its value being negative along half of the second reduced section are eliminated. By substituting $\cos\beta$ in Eq. (31), $b_2(\beta)$ is written as in the following:

$$b_2(\beta) = b_f - \left(\frac{b_2^2+4c_2^2}{4c_2}\right)\frac{(b_2+2c_2)(b_2-2c_2)}{\sqrt{(b_2-2c_2)^2(b_2+2c_2)^2+64c_2^2\left(x+a_1+b_1+a_2+\frac{b_2}{2}-\frac{L_b}{2}\right)^2}} + \left(\frac{b_2^2-4c_2^2}{4c_2}\right) \tag{35}$$

Ultimately, based on Eqs. (9), (17) and (35), the value of $\theta_2^{'}$ could be calculated using Eq. (36) as follows:

$$\theta_2^{'} = \frac{4M^{'}}{EL_b^2}\int_{\frac{L_b}{2}-a_1-b_1-a_2-b_2}^{\frac{L_b}{2}-a_1-b_1-a_2}\frac{x^2}{\frac{1}{12}\left[b_2(x)\left(h_w+2t_f\right)^3-(b_2(x)-t_w)h_w^3\right]}dx$$
$$= \frac{4M^{'}}{EL_b^2}\int_{\frac{L_b}{2}-a_1-b_1-a_2-b_2}^{\frac{L_b}{2}-a_1-b_1-a_2}\frac{x^2}{\frac{1}{12}\left[\left\{b_f-\left(\frac{b_2^2+4c_2^2}{4c_2}\right)\left(\frac{(b_2+2c_2)(b_2-2c_2)}{\sqrt{(b_2-2c_2)^2(b_2+2c_2)^2+64c_2^2\left(x+a_1+b_1+a_2+\frac{b_2}{2}-\frac{L_b}{2}\right)^2}}\right)\right\}.\left\{\left(h_w+2t_f\right)^3-h_w^3\right\}+\left(\frac{b_2^2-4c_2^2}{4c_2}\right)t_wh_w^3\right]}dx \tag{36}$$

By substituting Eqs. (8), (10), (12), (29) and (36) in Eq. (7), and assigning values to all the parameters involved, the value of $\theta^{'}_{B_R}$ could be calculated using the Maple software.

$$\theta^{'}_{B_L} = \theta^{'}_{B_R} \rightarrow \frac{\frac{P}{2}\cdot L_c^2}{2EI_c} - \frac{M^{'}L_c}{EI_c} = \theta^{'}_{B_R} \tag{37}$$

From Eq. (37), it can be seen that the bending moment in the presence of DRBS connections is dependent on the lateral force applied, beam length, column length, beam flange width, beam flange thickness, beam web depth, beam web thickness, the six DRBS connection parameters, and the modulus of elasticity of the cross-section or in other words, $M^{'} = f(P, L_b, L_c, b_f, t_f, h_w, t_w, a_1, a_2, b_1, b_2, c_1, c_2, E)$.

Using the compatibility equation and with a similar approach as that taken in the calculation of $\Delta_{Bending}$, the amount of elastic drift of the moment frame while considering the DRBS connections and only caused by the flexural deformations ($\Delta^{'}_{Bending}$) could be calculated as in the following:

$$\Delta^{'}_{Bending} = \frac{PL_c^3}{6EI_c} - \frac{M^{'}L_c^2}{2EI_c} \tag{38}$$

The effect of DRBS connections on the shear and axial deformations in the considered frame can be obtained by merely substituting the bending moment M with $M^{'}$ in Eqs. (3) and (4), respectively. Therefore, by adding up these two equations with Eq. (38), the total amount of elastic drift of the steel moment frame subjected to the lateral force P with DRBS connections and the same beam and column sections is calculated as follows:

$$\Delta^{'}_{Total} = \Delta^{'}_{Bending} + \Delta^{'}_{Shear} + \Delta^{'}_{Axial}$$
$$= \frac{PL_c^3}{6EI_c} - \frac{M^{'}L_c^2}{2EI_c} + \frac{P^2L_cL_b + 8M^{'2}}{2PL_bGA_s} + \frac{8M^{'2}L_c}{PL_b^2A_cE} \tag{39}$$

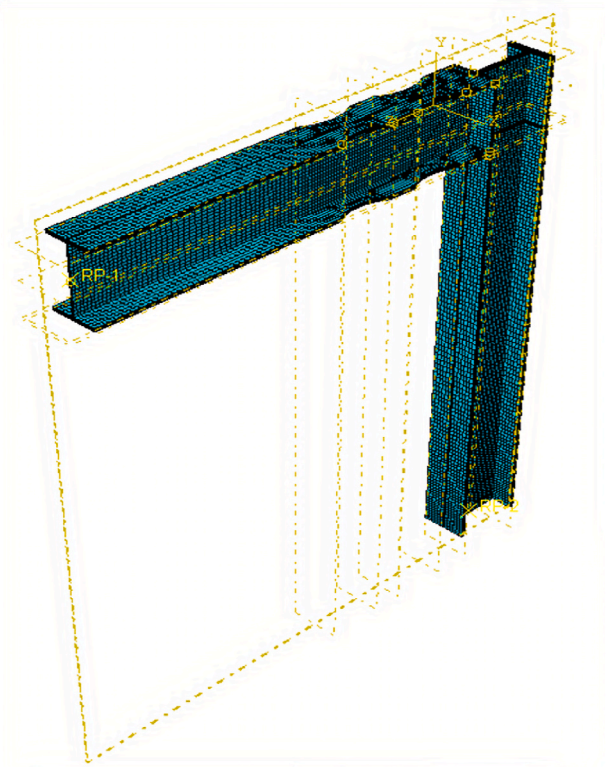

Fig. 10. The finite element mesh generated for the half-frame model.

Finally, the exact value of the elastic drift amplification factor in steel moment frames with DRBS connections is calculated using Eq. (40):

$$Am = \frac{\Delta'_{Total}}{\Delta_{Total}} = \frac{\frac{PL_c^3}{6EI_c} - \frac{M' L_c^2}{2EI_c} + \frac{P^2 L_c L_b + 8M'^2}{2PL_b GA_s} + \frac{8M'^2 L_c}{PL_b^2 A_c E}}{\frac{PL_c^3}{6EI_c} - \frac{ML_c^2}{2EI_c} + \frac{P^2 L_c L_b + 8M^2}{2PL_b GA_s} + \frac{8M^2 L_c}{PL_b^2 A_c E}} \quad (40)$$

3. Sensitivity analysis of the DRBS connection parameters

All of the geometrical parameters of the DRBS connection (a_1, b_1, c_1, a_2, b_2, and c_2) affect the amount of the elastic drift and lateral stiffness of steel moment frames, but the extent of their effect is different for each of these parameters. Hence, in this study, a sensitivity analysis using the response surface method (RSM) was conducted to determine the effect of each parameter involved. In this analysis, using the Maple software and Eq. (39), the effect of the parameters mentioned above on the elastic drift of the steel moment frame presented in Fig. 2, subjected to the lateral force of $P = 25$ ton, was investigated. The sensitivity analysis was conducted by selecting two HEA (500 and 1000) and two IPE (300 and 600) sections and considering the same limits for the DRBS connection parameters as those provided for the RBS connection parameters in ANSI/AISC 358-16 [22] (Eqs. (41)-(43)). During the analysis, the values of all parameters, except the one whose effect was being investigated, were kept constant and equal to the mean value of their corresponding acceptable ranges considered. The specifications of the selected beam and column sections and the steel used in the moment frame are presented in Tables 1 and 2, respectively.

$$0.5b_{bf} \le a_1, a_2 \le 0.75b_{bf} \quad (41)$$

$$0.65d \le b_1, b_2 \le 0.85d \quad (42)$$

$$0.1b_{bf} \le c_1, c_2 \le 0.25b_{bf} \quad (43)$$

Based on the results of the sensitivity analysis, presented in Figs. 6–9, the elastic drift of the moment frame increased with the increase in the DRBS connection parameters b_1, b_2, c_1, and c_2. In contrast, the increase in the parameters a_1 and a_2, led to a decrease in the amount of the elastic drift. In all cases, the observed changes in the amount of the elastic drift occurred in an approximately linear manner.

According to the slopes of the obtained graphs, it can be concluded that the parameters c_1 and c_2 have the most significant effect on the elastic drift of the steel moment frames with DRBS connections, followed by b_1, b_2, a_1, and ultimately a_2 in descending order, except in the case of the frame with the HEA1000 section, where a_1 has a more significant effect than b_1.

4. Finite element modeling and verification

4.1. Meshing

Since the loading applied in this study was of the static type, the default implicit solver of the utilized finite element software was used in the analyses conducted. The discretization was done using the continuum (solid) C3D8R element, an 8-noded reduced-integration linear brick element, which has one integration point in its center. The

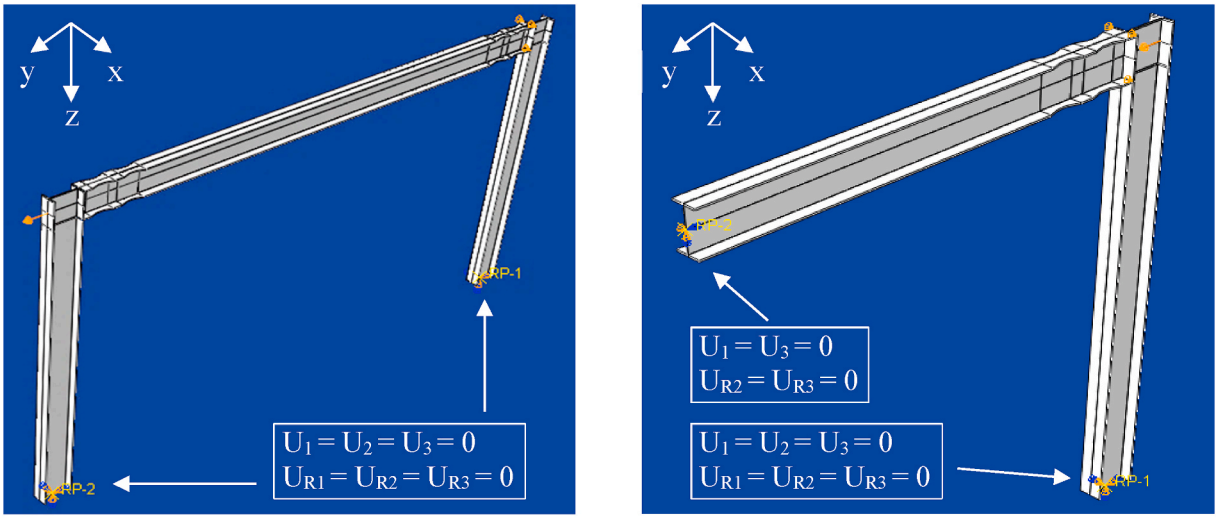

(a) Full-frame model (b) Half-frame model

Fig. 11. The boundary conditions and loading applied: (a) Full-frame model; (b) Half-frame model.

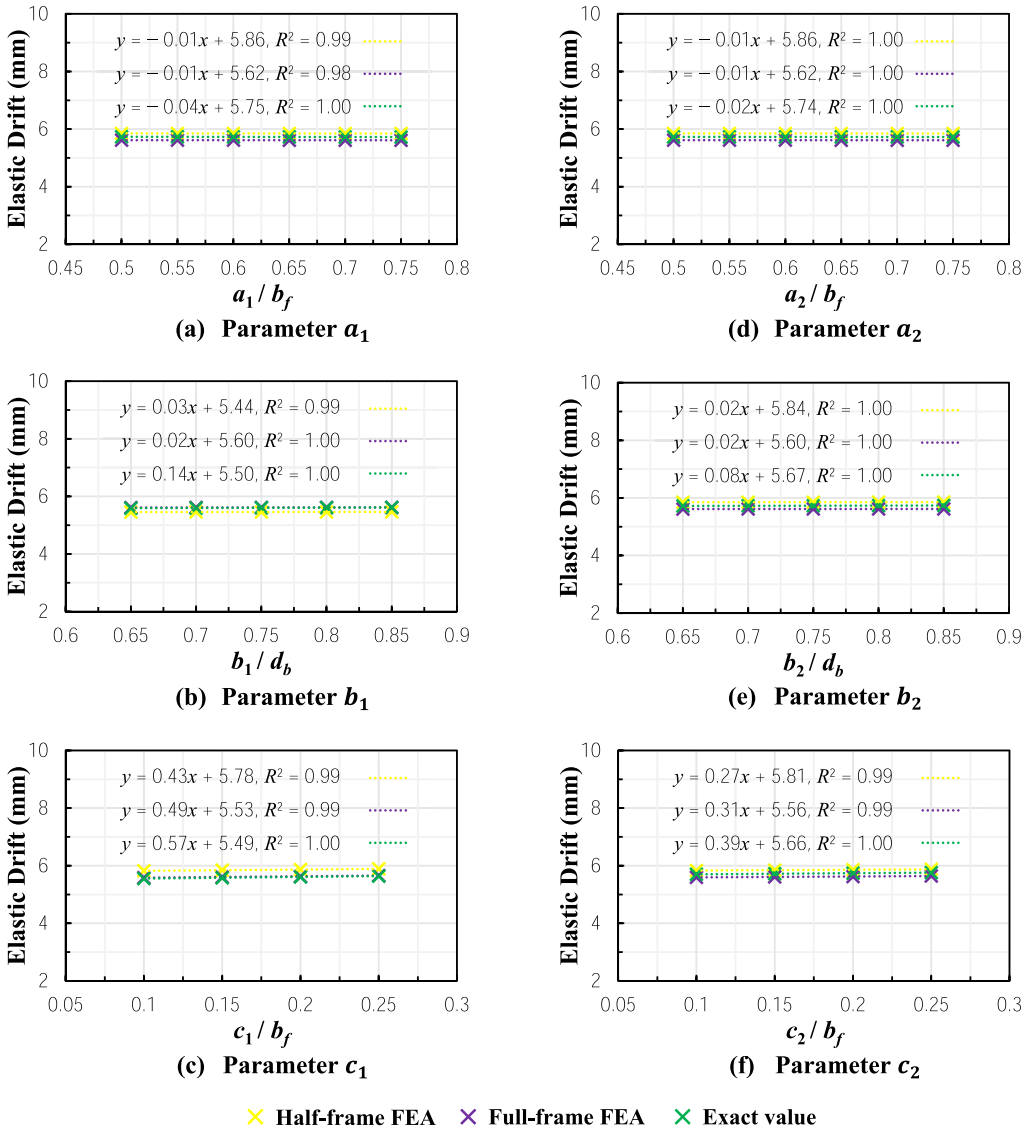

Fig. 12. Comparison of the results obtained for the frame with the HEA500 section: (a) Parameter a_1; (b) Parameter b_1; (c) Parameter c_1; (d) Parameter a_2; (e) Parameter b_2; (f) Parameter c_2.

minimum and maximum mesh sizes used for finite element modeling were equal to 1 and 2 cm, respectively. It should be noted that the connection details were not considered in generating the models, as the presence of the two cuts (the reduced sections) leads to reduced sensitivity at the connection region. Fig. 10 shows an example of the finite element meshes generated.

4.2. Boundary conditions and loading application

The modeling conducted in this study involved the two cases of the full-frame model and the half-frame model, which was considered according to analysis rules applicable to symmetrical structures. In the case of the half-frame model, the boundary conditions were applied as roller support at the free end of the half-beam and fixed support at the column base. In the case of the full-frame model, the boundary conditions were applied as fixed supports at the column bases. To simulate the abovementioned boundary conditions, the degrees of freedom of the nodes at the end of the half-beam and column bases were coupled to those of a reference node using a rigid body constraint. Such a constraint limits the displacements of the coupled nodes to those of a single rigid surface. The desired boundary conditions could thus be easily modeled by applying translational or rotational motion restrains in specific directions to the considered rigid surfaces.

The loading was applied to the considered models as a horizontal displacement equivalent to a 25-ton load, determined through interpolation. The boundary conditions and the loading applied to the models

Table 3
The geometric specifications of the frame with the HEA500 section.

t_f(cm)	b_f(cm)	t_w(cm)	h_w(cm)	I(cm^4)	A_s (cm^2)	A_c (cm^2)	L_b(m)	L_c(m)	a_1(cm)	b_1(cm)	c_1(cm)	a_2(cm)	b_2(cm)	c_2(cm)
2.3	30.0	1.2	44.4	86970	53	198	5.5	3.5	18.75	36.75	5.25	18.75	36.75	4.50

Table 4
Comparison of the elastic drift amplification factor values obtained using the method of virtual work and finite element analysis (HEA500 section).

Analysis type	Elastic drift (mm)	*Am*	Error (%)
Method of virtual work – With DRBS connections	5.719	1.029	0.29
Method of virtual work – Without DRBS connections	5.558		
Finite element analysis – With DRBS connections	5.844	1.012	
Finite element analysis – Without DRBS connections	5.773		

Table 5
The geometric specifications of the frame with the IPE600 section.

t_f(cm)	b_f(cm)	t_w(cm)	h_w(cm)	I(cm^4)	A_s(cm^2)	A_c(cm^2)	L_b (m)	L_c(m)	a_1(cm)	b_1(cm)	c_1(cm)	a_2(cm)	b_2(cm)	c_2(cm)
1.9	22.0	1.2	56.2	92080	67	156	5.7	3.8	13.75	45.00	3.85	13.75	45.00	2.20

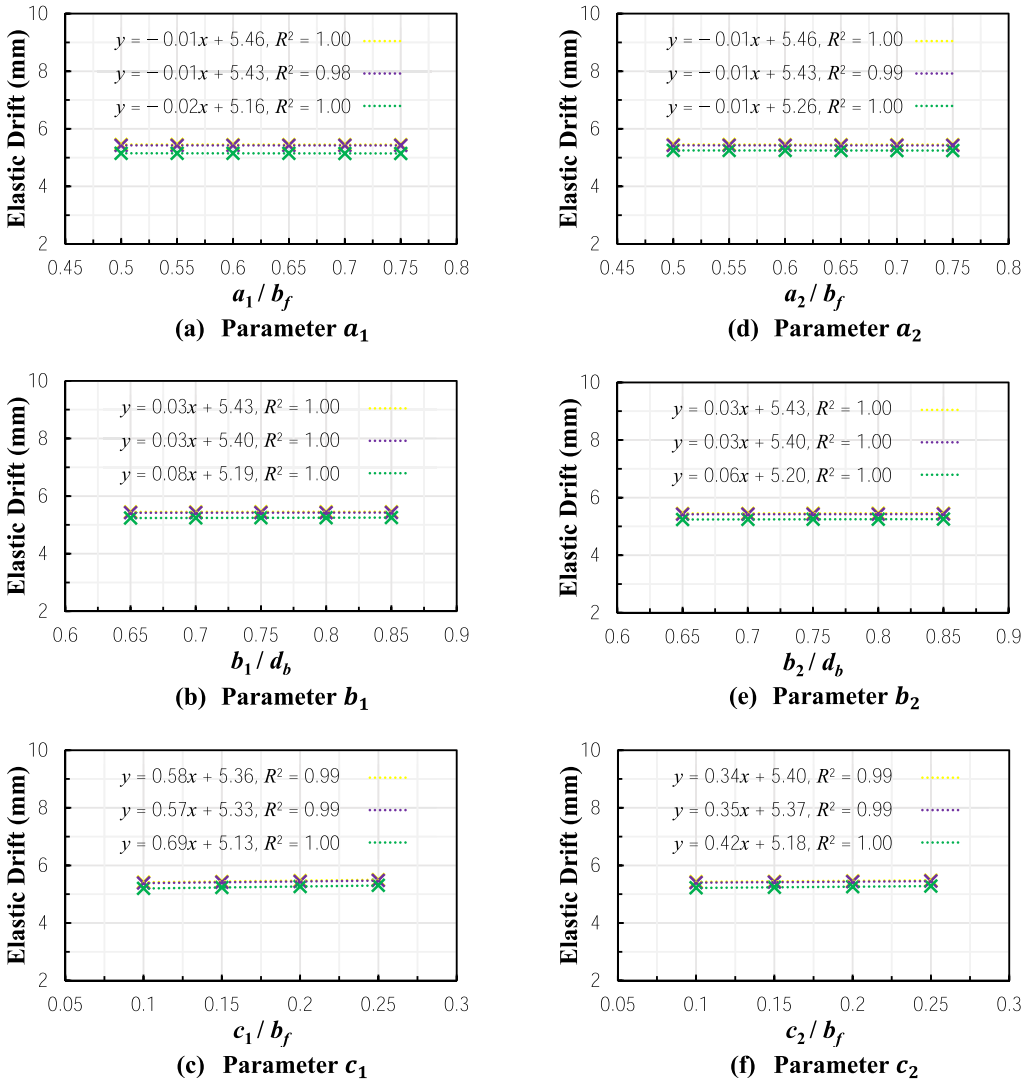

Fig. 13. Comparison of the results obtained for the frame with the IPE600 section: (a) Parameter a_1; (b) Parameter b_1; (c) Parameter c_1; (d) Parameter a_2; (e) Parameter b_2; (f) Parameter c_2.

Table 6
Comparison of the elastic drift amplification factor values obtained using the method of virtual work and finite element analysis (IPE600 section).

Analysis type	Elastic drift (mm)	*Am*	Error (%)
Method of virtual work – With DRBS connections	5.219	1.031	1.38
Method of virtual work – Without DRBS connections	5.063		
Finite element analysis – With DRBS connections	5.402	1.017	
Finite element analysis – Without DRBS connections	5.311		

Table 7
The specific first-order linear relationships derived for the elastic drift amplification factor in frames with DRBS connections made of HEA sections.

Section	Relationship	Section	Relationship	Average R^2
HEA100	$Am = 1 + 0.00425c_1 + 0.00388c_2$	HEA340	$Am = 1 + 0.00328c_1 + 0.00266c_2$	0.98
HEA120	$Am = 1 + 0.00392c_1 + 0.00365c_2$	HEA360	$Am = 1 + 0.00340c_1 + 0.00271c_2$	
HEA140	$Am = 1 + 0.00352c_1 + 0.00347c_2$	HEA400	$Am = 1 + 0.00328c_1 + 0.00266c_2$	
HEA160	$Am = 1 + 0.00360c_1 + 0.00347c_2$	HEA450	$Am = 1 + 0.00340c_1 + 0.00271c_2$	
HEA180	$Am = 1 + 0.00357c_1 + 0.00312c_2$	HEA500	$Am = 1 + 0.00366c_1 + 0.00277c_2$	
HEA200	$Am = 1 + 0.00349c_1 + 0.00317c_2$	HEA550	$Am = 1 + 0.00383c_1 + 0.00283c_2$	
HEA220	$Am = 1 + 0.00332c_1 + 0.00292c_2$	HEA600	$Am = 1 + 0.00562c_1 + 0.00127c_2$	
HEA240	$Am = 1 + 0.00314c_1 + 0.00301c_2$	HEA650	$Am = 1 + 0.00559c_1 + 0.00128c_2$	
HEA260	$Am = 1 + 0.00328c_1 + 0.00279c_2$	HEA700	$Am = 1 + 0.00553c_1 + 0.00130c_2$	
HEA280	$Am = 1 + 0.00331c_1 + 0.00283c_2$	HEA800	$Am = 1 + 0.00536c_1 + 0.00138c_2$	
HEA300	$Am = 1 + 0.00301c_1 + 0.00254c_2$	HEA900	$Am = 1 + 0.00501c_1 + 0.00135c_2$	
HEA320	$Am = 1 + 0.00314c_1 + 0.00260c_2$	HEA1000	$Am = 1 + 0.00457c_1 + 0.00137c_2$	

Table 8
The specific first-order linear relationships derived for the elastic drift amplification factor in frames with DRBS connections made of IPE sections.

Section	Relationship	Section	Relationship	Average R^2
IPE80	$Am = 1 + 0.00737c_1 + 0.00715c_2$	IPE270	$Am = 1 + 0.00664c_1 + 0.00555c_2$	0.98
IPE100	$Am = 1 + 0.00790c_1 + 0.00776c_2$	IPE300	$Am = 1 + 0.00591c_1 + 0.00537c_2$	
IPE120	$Am = 1 + 0.00788c_1 + 0.00734c_2$	IPE330	$Am = 1 + 0.00584c_1 + 0.00577c_2$	
IPE140	$Am = 1 + 0.00765c_1 + 0.00704c_2$	IPE360	$Am = 1 + 0.00621c_1 + 0.00489c_2$	
IPE160	$Am = 1 + 0.00766c_1 + 0.00766c_2$	IPE400	$Am = 1 + 0.00634c_1 + 0.00495c_2$	
IPE180	$Am = 1 + 0.00780c_1 + 0.00703c_2$	IPE450	$Am = 1 + 0.00654c_1 + 0.00570c_2$	
IPE200	$Am = 1 + 0.00688c_1 + 0.00659c_2$	IPE500	$Am = 1 + 0.00668c_1 + 0.00493c_2$	
IPE220	$Am = 1 + 0.00641c_1 + 0.00640c_2$	1PE550	$Am = 1 + 0.00682c_1 + 0.00462c_2$	
IPE240	$Am = 1 + 0.00700c_1 + 0.00619c_2$	IPE600	$Am = 1 + 0.00661c_1 + 0.00409c_2$	

Table 9
The formulae obtained for the estimation of the elastic drift amplification factor in frames with DRBS connections made of HEA sections.

Equation number	Formula	R^2
44	$Am = 1 + 0.00465c_1 + 0.00236c_2$	0.97
45	$Am = 1 + 0.00475c_1 + 0.00245c_2 - 0.00004c_1c_2$	0.97
46	$Am = 1 + 0.00074c_1^2 + 0.00049c_2^2$	0.50
47	$Am = 1 + 0.00111c_1^2 + 0.00086c_2^2 - 0.00081c_1c_2$	0.53
48	$Am = 1.001 + 0.00454c_1 + 0.00225c_2$	0.97
49	$Am = 1.004 + 0.00135c_1 + 0.00405c_2 + 0.00036c_1^2 - 0.00005c_1c_2 - 0.00016c_2^2$	0.98

generated are shown in Fig. 11.

4.3. Verification of the developed exact theoretical formulae and the sensitivity analysis

In order to verify the accuracy of the developed exact theoretical formulae and the sensitivity analysis conducted, it was necessary to compare the results with those obtained from the finite element modeling. For this purpose, the elastic drift and elastic drift amplification factor values obtained from the full-frame and half-frame finite element analyses and the adopted exact theoretical approach were evaluated against each other for the four sections HEA500, HEA1000, IPE300, and IPE600 with the specifications given in Tables 1 and 2

Fig. 12 shows the comparison of the results for the frame with the HEA500 section. The geometric specifications of the abovementioned frame are given in Table 3. Besides, Table 4 presents the comparison of the elastic drift amplification factor values obtained using the developed exact theoretical formulae (method of virtual work) and the finite element analysis.

The geometric specifications of the frame mentioned above are given

Table 10
The formulae obtained for the estimation of the elastic drift amplification factor in frames with DRBS connections made of IPE sections.

Equation number	Formula	R^2
50	$Am = 1 + 0.00665c_1 + 0.00526c_2$	0.93
51	$Am = 1 + 0.00792c_1 + 0.00653c_2 - 0.00069c_1c_2$	0.96
52	$Am = 1 + 0.00153c_1^2 + 0.00131c_2^2$	0.04
53	$Am = 1 + 0.00238c_1^2 + 0.00217c_2^2 - 0.00182c_1c_2$	0.07
54	$Am = 1.007 + 0.00564c_1 + 0.00425c_2$	0.97
55	$Am = 1.002 + 0.00634c_1 + 0.00764c_2 - 0.00052c_1^2 + 0.00780c_1c_2 - 0.00091c_2^2$	0.98

Table 11
The error values of the formulae presented in Table 9 for HEA sections with respect to the exact theoretical formula presented in Section 2.

Equation number	Minimum relative percentage error (%)	Maximum relative percentage error (%)	Mean absolute relative percentage error (%)
44	−0.78	0.39	0.13
45	−0.80	0.37	0.12
46	−1.63	1.24	0.60
47	−1.40	1.28	0.59
48	−0.78	0.40	0.12
49	−0.91	0.25	0.10

Table 12
The error values of the formulae presented in Table 10 for IPE sections with respect to the exact theoretical formula presented in Section 2.

Equation number	Minimum relative percentage error (%)	Maximum relative percentage error (%)	Mean absolute relative percentage error (%)
50	0.36	1.67	2.58
51	0.05	1.29	2.35
52	−0.08	1.99	3.27
53	−2.54	1.38	2.97
54	−0.29	1.31	2.30
55	0.19	2.15	3.68

in Table 5. Fig. 13 shows the comparison of the results for the frame with the IPE600 section. Also, Table 6 presents the comparison of the elastic drift amplification factor values obtained using the developed exact theoretical formulae (method of virtual work) and the finite element analysis.

The comparison of the elastic drift and the elastic drift amplification factor values from the finite element analysis of the modeled frames with the values obtained using the developed exact theoretical formulae indicated error values of less than 3%. These minimal error percentages prove the accuracy and precision of the theoretical formulae in calculating the exact amount of the elastic drift in moment frames with and without DRBS connections.

5. Deriving the specific elastic drift amplification factor relationships in frames with different HEA and IPE sections

Since c_1 and c_2 were found to have the most significant effect on the elastic drift of the moment frames analyzed among the six DRBS connection parameters, they were entered as the variables in the Design-Expert software. The acceptable ranges for c_1 and c_2 were considered the same as the limits defined by ANSI/AISC 358-16 [22] for the parameter c_1 in the RBS connection (Eq. (43)). The elastic drift was investigated in moment frames with DRBS connections made of two groups of beam and column sections. The first group included the sections ranging from HEA100 to HEA1000 and the second group included the sections ranging from IPE80 to IPE600. The elastic drift behavior of each of the considered frames was statistically analyzed with 13 points suggested by

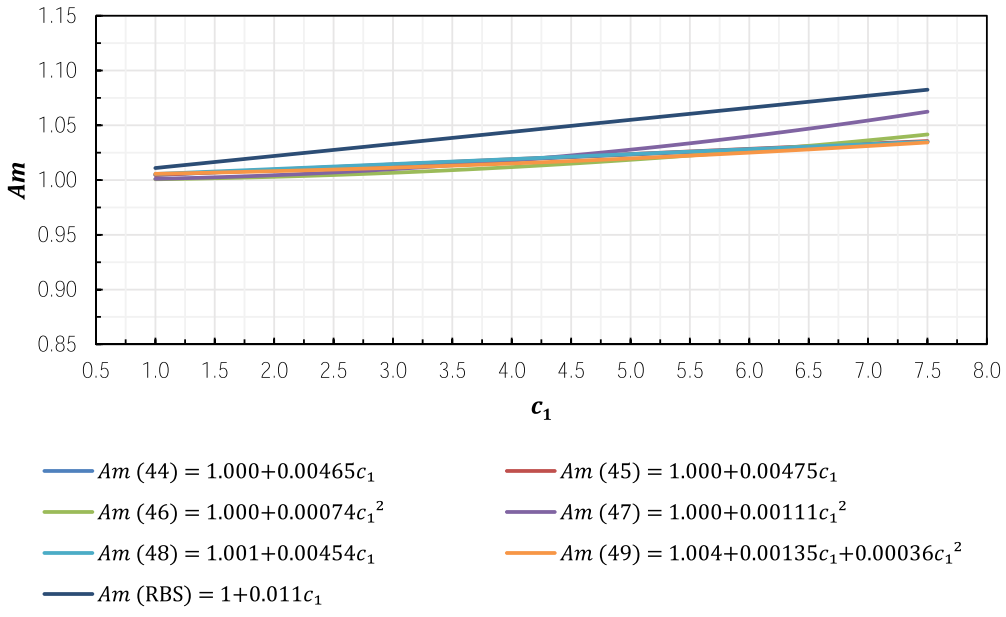

Fig. 14. Comparison graphs of the *Am* values obtained from Eq. (46) and (Fanaie et al. [18]) and the formulae proposed in this study (Table 9) when $c_2 = 0$.

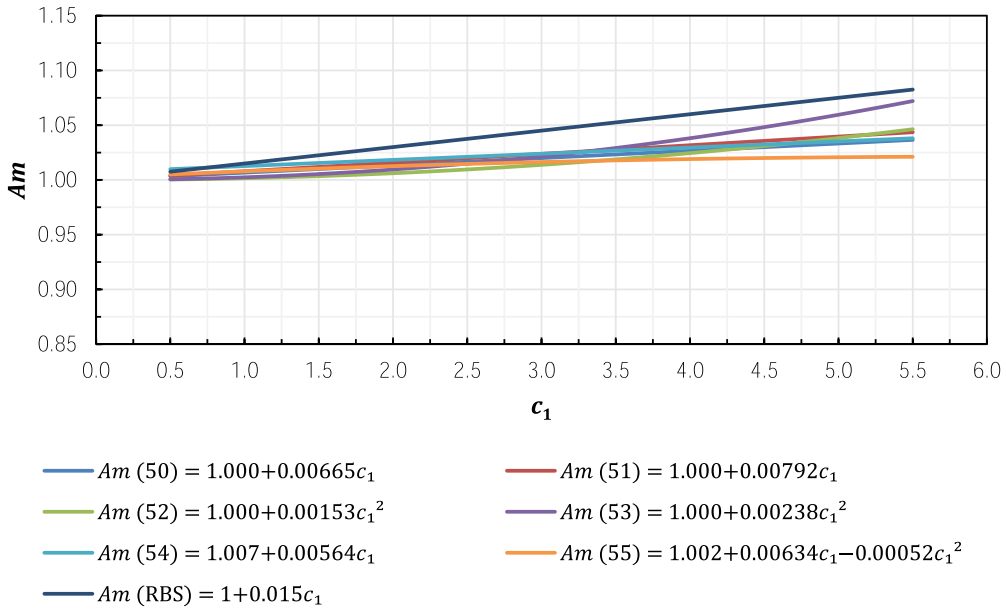

Fig. 15. Comparison graphs of the *Am* values obtained from Eq. (47) and (Fanaie et al. [18]) and the formulae proposed in this study (Table 10) when $c_2 = 0$.

Table 13
The error values of the formulae presented in Table 9 for HEA sections with respect to Eq. (46) when $c_2 = 0$.

Equation number	Minimum relative percentage error (%)	Maximum relative percentage error (%)	Mean absolute relative percentage error (%)
44	0.63	4.40	2.68
45	0.62	4.33	2.64
46	1.02	7.11	4.33
47	0.98	6.85	4.17
48	0.54	4.38	2.63
49	0.52	4.43	2.91

Table 14
The error values of the formulae presented in Table 10 for IPE sections with respect to Eq. (47) when $c_2 = 0$.

Equation number	Minimum relative percentage error (%)	Maximum relative percentage error (%)	Mean absolute relative percentage error (%)
50	0.38	4.24	2.50
51	0.32	3.60	2.12
52	0.65	3.44	2.82
53	0.64	2.26	1.88
54	−0.27	4.11	2.14
55	0.21	5.66	2.97

the Design-Expert software. The results were obtained as four relationships for each section considered.

The obtained coefficients of determination (the R^2 values) describe the percentage of the variance of the response, i.e., the elastic drift amplification of the moment frames studied, with the variance of the parameters c_1 and c_2 within their considered acceptable ranges. Based on the results, the first-order linear relationships derived exhibited higher coefficients of determination for both HEA and IPE groups and hence gave more precise response values. For a better presentation of the results, these first-order linear relationships are given in Tables 7 and 8.

6. Determination of the best formulae for the estimation of the elastic drift amplification factor in frames with HEA and IPE sections

In order to determine a single elastic drift amplification factor formula for each of the considered groups, the envelope curves of the relationships presented in Tables 7 and 8 were utilized to obtain two new sets of formulae for HEA and IPE sections. These new relationships, which are made up of terms with the coefficients c_1 c_2, c_1c_2, c_1^2, and c_2^2, are presented along with their corresponding R^2 values in Tables 9 and 10.

To find the best formula in each of the obtained sets, the accuracy of elastic drift amplification factor values from the relationships was assessed with respect to the exact values from the exact theoretical formula presented in Section 2. The results of the assessment are given in Tables 11 and 12.

According to the results, it can be concluded Eq. (44) is the best formula for estimating the elastic drift amplification factor in moment frames with DRBS connections constructed of HEA sections:

$$Am = 1 + 0.00465c_1 + 0.00236c_2 \tag{44}$$

It can also be concluded that equation number 51 is the best formula for estimating the elastic drift amplification factor in moment frames with DRBS connections constructed of IPE sections:

$$Am = 1 + 0.00792c_1 + 0.00653c_2 - 0.00069c_1c_2 \tag{45}$$

7. Comparison of the formulae obtained for frames with DRBS connections and the existing relationships for frames with RBS connections

Fanaie et al. [18] proposed Eqs. (46) and (47) for estimating the elastic drift amplification factor in moment frames with RBS connections constructed using HEA and IPE sections, respectively.

$$Am_{HEA} = 1 + 0.011c \tag{46}$$

$$Am_{IPE} = 1 + 0.015c \tag{47}$$

In order to investigate the accuracy of the formulae presented in Tables 9 and 10 in estimating the elastic drift amplification factor in moment frames with RBS connections, the *Am* values obtained from these formulae were compared to those given by Eqs. (46) and (47). For this purpose, the second reduced section was omitted, i.e., the value of c_2

was assumed to be equal to zero, and the value of c_1 was altered within the acceptable limits for each of the studied section groups.

Figs. 14 and 15 present the comparison graphs of the *Am* values obtained from Eqs. (46) and (47) (Fanaie et al. [18]) and the formulae proposed in this study (Tables 9 and 10). Tables 13 and 14 present the percentage error values of the formulae given in Tables 9 and 10 with respect to Eqs. (46) and (47). According to Tables 13 and 14, the maximum and minimum relative percentage error values and also the mean absolute relative percentage error values obtained for each of the formulae derived in this study are very small or, in other words, insignificant. However, according to Figs. 14 and 15, the existing relationships proposed by Fanaie et al. [18] resulted in greater *Am* values, indicating that the formulae of Tables 9 and 10 are rather not suitable for calculating the elastic drift in the moment frames with the conventional RBS connections.

8. Conclusions

In this research, the effect of the double reduced beam section (DRBS) connections on the stiffness of steel moment frames was investigated by presenting a theoretical approach based on mathematical relationships and structural analysis principles. To this end, first, based on geometric relationships and utilizing the method of virtual work, all of the shear, axial, and flexural deformations were taken into account to develop the exact formulae for calculating the elastic drift and the elastic drift amplification factor in a single-story single-span moment frame with DRBS connections. Next, by performing a sensitivity analysis, the most effective DRBS connection parameters on the elastic drift of the considered moment frame were determined. The accuracy of the developed exact theoretical formulae and the conducted sensitivity analysis was then evaluated using finite element modeling. In the next step, the response surface method (RSM) was utilized to derive highly accurate and specific relationships for the elastic drift amplification factor in moment frames made of different HEA and IPE sections. Ultimately, using the envelope curves of the developed relationships, two accurate and simple formulae based on DRBS connection parameters were proposed for estimating the elastic drift amplification factor in steel moment frames constructed of HEA and IPE sections. The following conclusions summarize the advantages of the presented methods and results obtained:

(1) This research presented an exact theoretical method, without simplifying assumptions and considering all the deformations involved, which could be used to determine the actual amount of elastic drift and the corresponding elastic drift amplification factor in moment frames with DRBS connections. Determining the exact value of the elastic drift amplification factor in moment frames with DRBS connections helps engineers optimally design the structures constructed using such frames and more accurately understand the elastic behavior of the newly developed DRBS connection.

(2) The results of the sensitivity analysis conducted to investigate the effect of the DRBS connection parameters on the elastic drift of moment frames showed that by increasing the values of parameters b_1, b_2, c_1, and c_2 in the DRBS connections, the elastic drift also increases in an approximately linear manner. Thus, it can be concluded that increasing the values of these DRBS parameters leads to a decrease in the stiffness of the corresponding moment frame. In contrast, the results showed that by increasing the values of parameters a_1 and a_2, the elastic drift decreases linearly. Hence, it can be concluded that increasing the values of these parameters increases the stiffness of the corresponding moment frame.

(3) The results of the conducted sensitivity analysis also showed that among the six DRBS connection parameters, the parameters c_1 and c_2 have the most significant effects on the elastic drift of considered moment frames with DRBS connections, followed by b_1, b_2, a_1, and ultimately a_2 in descending order, except in the case of the frame with the HEA1000 section, where a_1 has a more significant effect than b_1. In other words, the parameters c_1 and c_2 affect the stiffness of moment frames more significantly than the other DRBS connection parameters.

(4) The formulae derived using the RSM method for estimating the elastic drift amplification factor in moment frames with DRBS connections constructed of HEA and IPE sections exhibited nearly zero error relative to the exact theoretical results. Their coefficients of determination were also obtained to be approximately equal to 97%. Such results confirm the accuracy of these presented formulae in describing the elastic behavior of moment frames with DRBS connections.

(5) Among the derived relationships, Eqs. (44) and (45) were found to be the best simple formulae for estimating the elastic drift amplification factor in moment frames with DRBS connections constructed of HEA and IPE sections, respectively:

$$Am = 1 + 0.00465c_1 + 0.00236c_2$$

$$Am = 1 + 0.00792c_1 + 0.00653c_2 - 0.00069c_1c_2$$

Noting that precisely modeling DRBS connections in advanced scientific finite element software such as Abaqus is a time-consuming, inefficient procedure and that specialized commercial structural design software such as ETABS do not provide an option for directly modeling DRBS connections, these formulae can be utilized by practicing engineers to accurately estimate the elastic drift amplification factor when designing moment frames with DRBS connections in an efficient and fast manner based on the cut parameters c_1 and c_2.

(6) Based on the results obtained, the amount of the elastic drift amplification factor varied between 0 and 14.7% and between 0 and 5.5% in frames with HEA and IPE sections, respectively.

This study presented a theoretical investigation of the elastic behavior of steel moment frames incorporating the newly proposed DRBS connection. Results obtained herein and those from previously conducted numerical studies suggest that this design has an acceptable behavior and could be utilized as an improved alternative to the conventional RBS connection. Nevertheless, it should be emphasized that an experimental study is still necessary to evaluate the exact seismic performance of moment frames with DRBS connections more comprehensively. Hence, further research in this field can be focused on laboratory testing of DRBS connection specimens to observe the sequence of the intended plastic hinge formation in frames with such connections. The DRBS connection could indeed be added to the category of prequalified connections for steel moment frames and readily used in the construction industry in case future experimental studies confirm its promising seismic performance suggested by numerical and theoretical results.

CRediT authorship contribution statement

Nader Fanaie: Conceptualization, Methodology, Supervision, Writing original draft.

Zahra Nadalipour: Investigation, Data curation, Software, Validation.

Omid Sepasgozar Sarkhosh: Visualization, Writing original draft, Writing Review & editing.

Shervin Safaei Faegh: Methodology, Software.

Declaration of competing interest

The authors declare that they have no known competing financial interests or personal relationships that could have appeared to influence the work reported in this paper.

References

[1] D.T. Pachoumis, E.G. Galoussis, C.N. Kalfas, I.Z. Efthimiou, Cyclic performance of steel moment-resisting connections with reduced beam sections - experimental analysis and finite element model simulation, Eng. Struct. (2010), https://doi.org/10.1016/j.engstruct.2010.04.038.

[2] A. Sivandi-Pour, Performance assessment of steel moment connections retrofitted with various reduced section patterns, Civ. Environ. Eng. Rep. (2019), https://doi.org/10.2478/ceer-2019-0041.

[3] R. Rahnavard, A. Hassanipour, N. Siahpolo, Analytical study on new types of reduced beam section moment connections affecting cyclic behavior, Case Stud. Struct. Eng. (2015), https://doi.org/10.1016/j.csse.2015.03.001.

[4] A. Plumier, New idea for safe structures in seismic zones, in: IABSE Symposium-Mixed Structures Including New Materials, International Association for Bridge and Structural Engineering, Brussels, Belgium, 1990.

[5] S.J. Chen, C.H. Yeh, J.M. Chu, Ductile steel beam-to-column connections for seismic resistance, J. Struct. Eng. (1996), https://doi.org/10.1061/(ASCE)0733-9445(1996)122:11(1292).

[6] M.D. Engelhardt, T. Winneberger, A.J. Zekany, T.J. Potyraj, Experimental investigation of dogbone moment connections, Eng. J. (1998).

[7] A. Plumier, The dogbone: back to the future, Eng. J. (1997).

[8] E. Paul Popov, T.S. Yang, S.P. Chang, Design of steel MRF connections before and after 1994 Northridge earthquake, Eng. Struct. (1998), https://doi.org/10.1016/S0141-0296(97)00200-9.

[9] Q. Yang, B. Li, N. Yang, Aseismic behaviors of steel moment resisting frames with opening in beam web, J. Constr. Steel Res. (2009), https://doi.org/10.1016/j.jcsr.2009.01.007.

[10] S.L. Jones, G.T. Fry, M.D. Engelhardt, Experimental evaluation of cyclically loaded reduced beam section moment connections, J. Struct. Eng. (2002), https://doi.org/10.1061/(ASCE)0733-9445(2002)128:4(441).

[11] M. TahamouliRoudsari, A.R. Moradi Garoosi, A. Alipour, M. Torkaman, H. Moghadam Abrishami, M. Rambarzini, A. Doudman Koushki, S. Khodaparast, S. Bonyadirad, Comparing the Seismic Performances of Shallow Beam Connections with Accordion Webs and Reduced Sections: an Experimental Study, Structures, 2019, https://doi.org/10.1016/j.istruc.2019.10.014.

[12] R. Montuori, The influence of gravity loads on the seismic design of RBS connections, Open Construct. Build Technol. J. (2015), https://doi.org/10.2174/1874836801408010248.

[13] M. Tahamouli Roudsari, H. Jamshidi K, F. Akbari G, M. Torkaman, An experimental and numerical investigation of reduced beam section connections with horizontal and vertical web stiffeners, Asian J. Civ. Eng. (2020), https://doi.org/10.1007/s42107-019-00214-1.

[14] A.R. Moradi Garoosi, M. TahamouliRoudsari, B. Hosseini Hashemi, Experimental evaluation of rigid connection with reduced section and replaceable fuse, Structures (2018), https://doi.org/10.1016/j.istruc.2018.11.010.

[15] R. Montuori, V. Sagarese, The use of steel rbs to increase ductility of wooden beams, Eng. Struct. (2018), https://doi.org/10.1016/j.engstruct.2018.05.024.

[16] M.A. Morshedi, K.M. Dolatshahi, S. Maleki, Double reduced beam section connection, J. Constr. Steel Res. (2017), https://doi.org/10.1016/j.jcsr.2017.07.013.

[17] B. Sai Chandana, C. Arunkumar, N. Umamaheswari, Experimental and numerical investigation on the moment rotation behavior of cruciform moment connections with reduced beam sections, J. Inst. Eng. Ser. A (2020), https://doi.org/10.1007/s40030-019-00410-x.

[18] N. Fanaie, S.S. Faegh, F. Partovi, An improved and innovative formulation for calculating amplified elastic story drift induced by RBS connections in steel moment frames, J. Constr. Steel Res. (2019), https://doi.org/10.1016/j.jcsr.2019.06.003.

[19] J.J. Chambers, S. Almudhafar, F. Stenger, Effect of reduced beam section frame elements on stiffness of moment frames, J. Struct. Eng. (2003), https://doi.org/10.1061/(ASCE)0733-9445(2003)129:3(383).

[20] C.H. Lee, S.W. Chung, A simplified analytical story drift evaluation of steel moment frames with radius-cut reduced beam section, J. Constr. Steel Res. (2007), https://doi.org/10.1016/j.jcsr.2006.06.031.

[21] Federal Emergency Management Agency (FEMA), FEMA 350 Recommended Seismic Design Criteria for New Steel Moment Frame Buildings, Federal Emergency Management Agency (FEMA), Washington, DC, 2000.

[22] American Institute of Steel Construction (AISC), ANSI/AISC 358-16 Prequalified Connections for Special and Intermediate Steel Moment Frames for Seismic Applications, American Institute of Steel Construction (AISC), Chicago, IL, 2016.